CHEMICAL SYSTEMS LABORATORY CONTRACTOR REPORT

ARCSL-CR-82020

ELONGATIONAL VISCOSITY RHEOLOGICAL PARAMETER STUDY

by

Stanley Middleman

June 1982

THE UNIVERSITY OF CALIFORNIA, SAN DIEGO

Department of Applied Mechanics and Engineering Sciences

La Jolla, California 92093

Contract No. DAAK-11-80-C-0001

US ARMY ARMAMENT RESEARCH AND DEVELOPMENT COMMAND
Chemical Systems Laboratory
Aberdeen Proving Ground, Maryland 21010

Disclaimer

The views, opinions and/or findings contained in this report are those of the authors and should not be construed as an official Department of the Army position, policy, or decision unless so designated by other documentation.

Disposition

Destroy this report when it is no longer needed. Do not return to the originator.

UNCLASSIFIED

SECURITY CLASSIFICATION OF THIS PAGE (When Data Entered)

REPORT DOCUMENTATION PAGE		READ INSTRUCTIONS BEFORE COMPLETING FORM
1. REPORT NUMBER ARCSL-CR-82020	2. GOVT ACCESSION NO. AD A125265	3. RECIPIENT'S CATALOG NUMBER
4. TITLE (and Subtitle) ELONGATIONAL VISCOSITY RHEOLOGICAL PARAMETER STUDY		5. TYPE OF REPORT & PERIOD COVERED Contractor Report October 1979 to December 1981 6. PERFORMING ORG. REPORT NUMBER
7. AUTHOR(s) Stanley Middleman		8. CONTRACT OR GRANT NUMBER(s) DAAK-11-80-C-0001
9. PERFORMING ORGANIZATION NAME AND ADDRESS The Regents of the University of California University of California, San Diego Urey Hall, La Jolla, California 92093		10. PROGRAM ELEMENT, PROJECT, TASK AREA & WORK UNIT NUMBERS 1L162706A553, Area 3-D
11. CONTROLLING OFFICE NAME AND ADDRESS Commander/Director, Chemica Systems Laboratory ATTN: DRDAR-CLB-PO Aberdeen Proving Ground, Maryland 21010		12. REPORT DATE June 1982 13. NUMBER OF PAGES 71
14. MONITORING AGENCY NAME & ADDRESS (if different from Controlling Office) Commander/Director, Chemical Systems Laboratory ATTN: DRDAR-CLJ-R Aberdeen Proving Ground, Maryland 21010		15. SECURITY CLASS. (of this report) UNCLASSIFIED 15a. DECLASSIFICATION/DOWNGRADING SCHEDULE N/A

16. DISTRIBUTION STATEMENT (of this Report)

Approved for public release, distribution unlimited.

17. DISTRIBUTION STATEMENT (of the abstract entered in Block 20, if different from Report)

18. SUPPLEMENTARY NOTES

Contract Officers Representative: Mr. Raymond Tytus, DRDAR-CLB-PO, 301-671-3321

19. KEY WORDS (Continue on reverse side if necessary and identify by block number)

Viscoelastic liquid	Fluid rheometer
Elongational viscosity	Gas bubble collapse
Bulk liquid breakup	Elongation rate
Drop deformation	Radius collapse rate

20. ABSTRACT (Continue on reverse side if necessary and identify by block number)

The physics of drop breakup is considered, and an analysis suggests that the elongational viscosity of the drop may control its disruption to smaller droplets. An experimental system has been designed which permits the study of the elongational rheology of liquids of interest. In the experiment, the rate of collapse of a gas bubble within the test liquid is measured. Preliminary data are obtained which indicate the feasibility of performing a precise experiment. Features of the experimental system that require improvement are pointed out and discussed.

DD FORM 1 JAN 73 1473 EDITION OF 1 NOV 65 IS OBSOLETE

UNCLASSIFIED

SECURITY CLASSIFICATION OF THIS PAGE (When Data Entered)

PREFACE

The work described in this report was authored under Contract Number DAAK-11-80-C-0001, Project Number 1L162706A553, Technical Area 3-D, titled Chemical Systems and Procedures Technology. This work was performed between October 1979 and December 1981.

The use of trade names in this report does not constitute an official endorsement or approval of the use of such commercial hardware of software. This report may not be cited for purposes of advertisement.

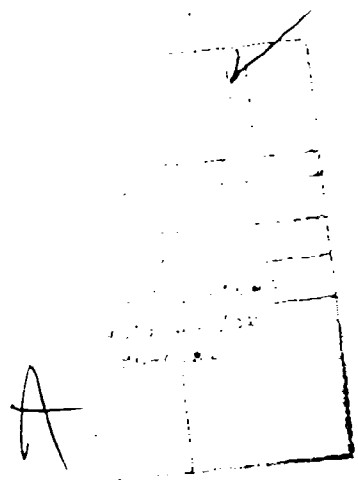

CONTENTS

1.	INTRODUCTION	7
2.	PREVIOUS RELEVANT RESEARCH	9
3.	A MODEL FOR DISK DEFORMATION	10
4.	BUBBLE COLLAPSE AS AN ELONGATIONAL FLOW	16
5.	EXPERIMENTAL DESIGN	21
6.	THE EXPERIMENTAL SYSTEM	29
7.	CALIBRATION AND ANALYSIS OF EXPERIMENTAL DATA	45
8.	EXPERIMENTAL DATA	46
9.	EVALUATION AND DISCUSSION OF DATA	48
10.	RECOMMENDATIONS	51
	LITERATURE CITED	55
	APPENDIX	57
	GLOSSARY	65
	DISTRIBUTION LIST	67

LIST OF FIGURES

1.	Schematic Showing the Deformation of Disk Under a Squeezing Pressure.	11
2.	Pressure Required to Squeeze a Disk at a Fixed Rate.	17
3.	Solutions of the Rayleigh Equation for a Newtonian Liquid.	28
4.	Schematic of the Experimental System.	30

5.	Photograph of the Apparatus.	31
6.	Schematic of the Test Cell.	32
7.	Photograph of the Test Cell.	33
8.	Schematic of the Electrode.	34
9.	Typical Streak Photograph of Bubble Collapse.	41
10.	Complex Viscosity Data for Solutions Studied.	43
11.	Dynamic Moduli Data for Solutions Studied.	44
12.	Still Photograph of a Stationary Bubble.	47
13.	Data for Two Collapse Events.	49

ELONGATIONAL VISCOSITY RHEOLOGICAL PARAMETER STUDY

1. INTRODUCTION

The following objectives were set under this research contract:

a. To establish a hypothesis relating the deformation of Newtonian and viscoelastic liquids to an elongational viscosity parameter

b. To design and develop a technique to determine this parameter for a series of liquids over an extended range of elongation rates.

These objectives were aimed at elucidating the process of dispersion of a liquid into droplets, and the role that liquid properties play in affecting that process.

For a variety of circumstances it may be desirable to take a coherent mass of liquid and cause it to be distributed into a spray or cloud of fine particles. The ultimate disposition of this cloud, its spatial dispersion, settling velocity, and ultimately its interaction with surrounding surfaces, depends strongly upon the particle size distribution created by the breakup mechanism. The particle size distribution depends upon the mechanism used to form the initial cloud, and upon the physical properties of the liquid mass. It is well recognized that surface tension is a primary liquid property affecting drop breakup. In viscous liquids one observes that the liquid viscosity exerts an effect on drop size. In liquids containing polymeric modifiers it has become clear that an additional property, related in some way to viscoelastic behavior, is necessary in order to

describe breakup characteristics. It is by no means clear, however, what property one needs to measure. The primary goals of this program are to clarify this last point.

A significant literature exists in the general area of drop breakup by high velocity airstreams.[1-10] All of these studies suggest that drop breakup involves two mechanisms: ligament formation associated with pressure and velocity fluctuations, and drop formation by Rayleigh instability of the ligaments.

Ligament formation would appear to be one mechanism that determines drop size. Thus, it is necessary to develop an understanding of the role played by fluid properties in affecting the ease with which some energetic mechanism can "pull" ligaments from the main body of the liquid mass.

One may regard ligament formation as a stretching flow, similar to that in which a cylindrical specimen of material is elongated as a cylinder of increasing length and decreasing diameter. Because this is an elongational flow, and not a shearing flow, it is the elongational rheology of the liquid that plays the major role in determining the resistance of an element of liquid to ligament formation.

In the past, elongational rheology studies have been restricted to molten polymers or rubbery elastomers of sufficiently high viscosity (greater than 10^6 poise) that can be formed into a cylindrical specimen and pulled in a stress-strain type of test. The liquids of interest here are of relatively

low viscosity (typically 10 to 100 centipoise) and cannot be formed into a specimen. The challenging task at hand, then, is the development of a test procedure which provides a measure of the elongational rheology of such liquids.

We examine, first, some simple models of drop deformation under conditions that would suggest the importance of elongational viscosity. Then we describe the principles of the technique proposed for the measurement of elongational response of a liquid. Progress toward creation of an apparatus for performing this measurement is then described.

2. PREVIOUS RELEVANT RESEARCH

The most relevant studies are cited in the list of references.[1-10] The generally agreed upon picture that emerges is the following: a mass of liquid is first pulled into ligaments which break down to large drops. Subsequently, a droplet undergoes two important events. The first is acceleration of the drop, which may lead to Taylor instability of the surface. It would appear that a criterion of breakup through this mechanism depends upon the bond number

$$Bo = g \rho r_o^2 / \sigma \qquad (1)$$

where g is the drop acceleration

ρ is the drop density

r_o is the drop radius

σ is the interfacial tension

We note that this criterion does not involve any rheological parameter.

The second event of importance is the deformation of the drop into a thin disk. Studies cited suggest that the disk may deform into a "bag" which then disintegrates into droplets. Alternatively, some studies indicate that liquid is stripped from the rim of the disk. In either case disk formation is central to this mode of breakup.

In what follows we model the process of drop deformation into a thin disk, and suggest that the presence of polymeric additives retards this deformation. We show that disk formation is an elongational flow. Thus we hypothesize that elongational rheology is central to the deformation process, and that it is reasonable to seek a connection between elongational rheology and drop breakup.

3. A MODEL FOR DISK DEFORMATION

To provide a tractable problem we take the following model. The spherical drop is replaced by a cylinder of equal length and diameter (see Figure 1). At some initial instant $t = 0$ a uniform pressure is imposed on the circular faces of the disk, causing it to deform into a thinner disk. We neglect the viscosity of the surrounding air.

Newtonian fluid:

$$\text{Continuity equation} \quad \frac{1}{r}\frac{\partial}{\partial r}(r v_r) + \frac{\partial v_z}{\partial z} = 0 \qquad (2)$$

Assume a solution with properties

(a)

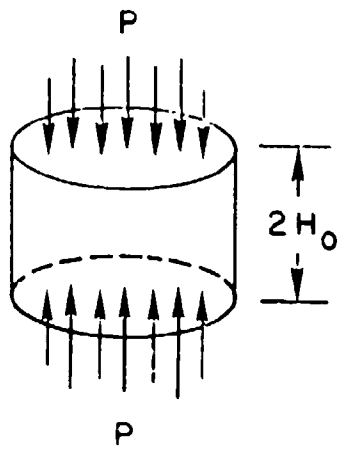

(b)

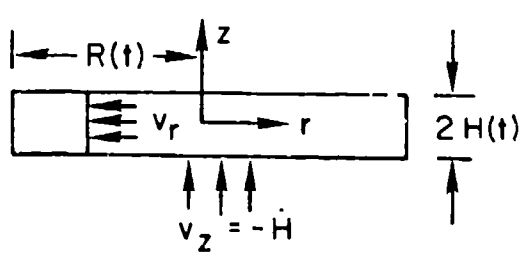

Figure 1

$$v_z = v_z(z) \tag{3}$$

$$v_r = r f(z) \tag{4}$$

$$p = \text{constant} = P \tag{5}$$

Neglecting disk inertia we find the radial momentum equation that must be satisified to take the form

$$\frac{\partial^2 v_r}{\partial z^2} = 0 \tag{6}$$

A solution satisfying these equations is

$$v_r = \alpha r \tag{7}$$

where we have assumed that no shear stress is exerted by the surrounding inviscid gas:

$$\tau_{rz} = 0 = \frac{\partial v_r}{\partial z} \tag{8}$$

The equation of continuity is integrated to yield

$$2\pi r \int_0^H v_r \, dz + \pi r^2 H = 0 \tag{9}$$

from which it follows that

$$\alpha = \frac{1}{2} \frac{(-\dot{H})}{H} \, . \tag{10}$$

Here, H is the half-thickness of the disk at any time t, and $(-\dot{H})$ is half the rate of thinning.

In order to use realistic (and therefore, complex) constitutive equations it is necessary to consider the fluid motion in detail through the components of the deformation tensor $\chi_{[o]}$.[11] We begin by considering the coordinates r', z' of an element of fluid at time t'. Then we have

$$v'_r = \frac{\partial r'}{\partial t'} = \alpha r' \tag{11}$$

$$v'_z = \frac{\partial z'}{\partial t'} = -2\alpha z' \tag{12}$$

Assuming that α is an unknown function of time, but not of position, we have, upon integrating Eqs. 11 and 12,

$$r' = C \exp \int \alpha \, dt' \tag{13}$$

where C is an integration constant.

Using

$$\alpha = -\frac{1}{2}\frac{\dot{H}}{H} = -\frac{1}{2}\frac{d \ln H}{dt} \tag{14}$$

we may write this as

$$r' = C \exp \int -\frac{1}{2}\frac{d \ln H'}{dt'} dt'$$

$$= C \exp \int -\frac{1}{2} d \ln H'$$

or

$$r' = C H'^{-\frac{1}{2}} \tag{15}$$

To find C we use the condition that $r' = r$ at $t' = t$, where $H' = H$; this gives

$$\frac{r'}{r} = \left[\frac{H(t)}{H'(t')}\right]^{\frac{1}{2}} \tag{16}$$

In a similar manner we find

$$\frac{z'}{z} = \frac{H'(t')}{H(t)} \tag{17}$$

The components of $\underset{\sim}{\gamma}'_{[o]}$ are found using[11]

$$\gamma'_{[o]rr} = 1 - \left(\frac{dr}{dr'}\right)^2 = 1 - \frac{H'}{H} \tag{18}$$

$$\gamma'_{[o]\theta\theta} = 1 - \left(\frac{r}{r'}\right)^2 = \gamma_{[o]rr} \tag{19}$$

$$\gamma'_{[o]zz} = 1 - \left(\frac{dz}{dz'}\right)^2 = 1 - \left(\frac{H}{H'}\right)^2 \tag{20}$$

The pressure causing the deformation, P, may be written as

$$P = -T_{zz} = -\left(\tau_{zz} - \tau_{rr}\right) \tag{21}$$

where we assume $T_{rr} = 0$.

Now we must introduce some realistic viscoelastic constitutive equation. Related studies in our laboratories[12] suggest that a useful model is the integral model due to Wagner

$$\underset{\sim}{\tau} = \int_{-\infty}^{t} M(t - t') \, \underset{\sim}{\gamma}_{[o]} \, dt' \tag{22}$$

where M is some appropriate memory function.

$$P = \tau_{rr} - \tau_{zz} = \int_{-\infty}^{t} M(t - t') \left(\gamma'_{[o]rr} - \gamma'_{[o]zz} \right) dt' \tag{23}$$

$$= \int_{-\infty}^{t} M(t - t') \left[\left(\frac{H}{H'} \right)^2 - \left(\frac{H'}{H} \right) \right] dt'$$

The simplest case to examine, computationally, and one that suffices to illustrate the role of elongational rheology in disk deformation, seeks the pressure required to achieve a specified rate of thinning. Thus we assume

$$-\dot{H}/H = \dot{\epsilon}_o = \text{constant} \tag{24}$$

and find, upon integrating Eq. 23, that

$$\pi(T; \Lambda) = \frac{2}{1 - 2\Lambda} \left\{ 1 - \exp \left[- \left(1 - 2\Lambda \right) T \right] \right\}$$

$$- \frac{1}{1 + \Lambda} \left\{ 1 - \exp \left[- \left(1 + \Lambda \right) T \right] \right\} \tag{25}$$

We have defined the following dimensionless groups:

$$\pi = P(t)/\mu \dot{\epsilon}_o$$

$$\Lambda = \lambda \dot{\epsilon}_o$$

$$T = t/\lambda$$

We have chosen $M(t - t')$ to take the form

$$M = \frac{\mu}{\lambda^2} \exp\left[- (t - t')/\lambda \right] \tag{26}$$

which corresponds to the codeformational Maxwell fluid.[11]

Figure 2 shows $\Pi(T, \Lambda)$ versus T. For the Newtonian fluid, obtained from Eq. 26 as the limit when $\lambda \to 0$, we find

$$\Pi_N \equiv 1 \qquad \text{for all time} \tag{27}$$

Figure 2 demonstrates that, in order to maintain the same thinning rate $\dot{\epsilon}_o = - \dot{H}/H$ as a Newtonian fluid with the same shear viscosity μ, one would have to impose a larger pressure P on this viscoelastic fluid. This phenomenon arises not from viscoelasticity per se, but from the elongational viscosity function associated with this particular fluid.

We conclude that an elongational viscosity of the type often identified with polymer solutions exerts a retarding influence on the thinning rate of a liquid disk subjected to a uniform pressure. Thus, elongational viscosity may play an important role in controlling events which are believed to lead to droplet disruption.

4. BUBBLE COLLAPSE AS AN ELONGATIONAL FLOW

Earlier studies[13-15] have established that the flow field in a liquid surrounding a spherical collapsing bubble is an elongational flow. This

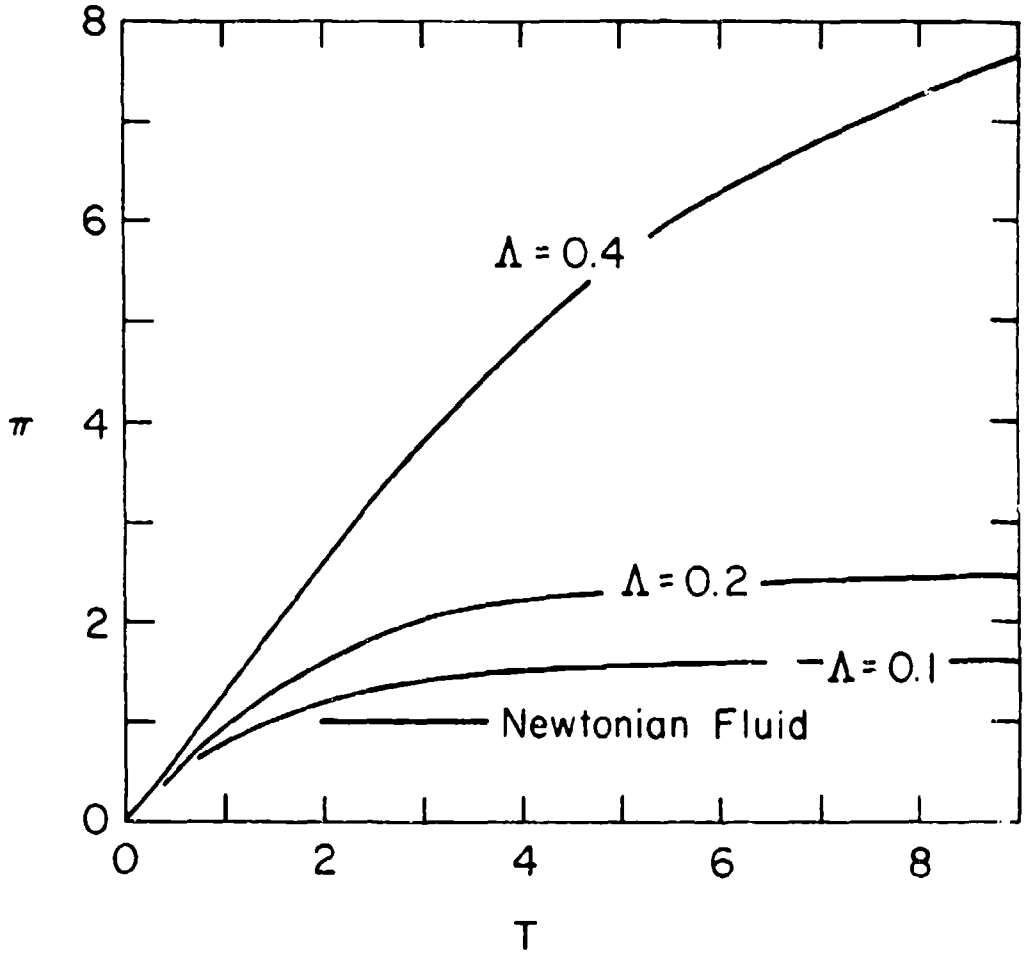

Figure 2

follows directly from the kinematics, defined by the continuity equation in spherical coordinates. Assuming spherically symmetric collapse, one integrates

$$\frac{\partial}{\partial r} r^2 v_r = 0 \tag{28}$$

to find

$$v_r = \frac{\dot{R} R^2}{r^2} = \frac{A(t)}{r^2} \tag{29}$$

where $\dot{R} = dR/dt$ is the rate of change of bubble radius. It is useful to note, at this point, that we may write

$$A(t) = \dot{R} R^2 = \frac{1}{3} \frac{d}{dt} R^3 \tag{30}$$

The rate of deformation tensor $\underset{\sim}{\Delta}$ takes the form

$$\underset{\sim}{\Delta} = \begin{pmatrix} \frac{\partial v_r}{\partial r} & 0 & 0 \\ 0 & \frac{v_r}{r} & 0 \\ 0 & 0 & \frac{v_r}{r} \end{pmatrix} = \dot{\epsilon} \begin{pmatrix} 2 & 0 & 0 \\ 0 & -1 & 0 \\ 0 & 0 & -1 \end{pmatrix} \tag{31}$$

where

$$\dot{\epsilon} = -2R^2 R/r^3 \tag{32}$$

The components of $\underset{\sim}{\gamma}'_{[o]}$ are given[11]

$$\underset{\sim}{\gamma}'_{[o]} = \begin{pmatrix} 1 - \left(\frac{\partial r}{\partial r'}\right)^2 & 0 & 0 \\ 0 & 1 - \left(\frac{r}{r'}\right)^2 & 0 \\ 0 & 0 & 1 - \left(\frac{r}{r'}\right)^2 \end{pmatrix} \tag{33}$$

Here, r and r' are the radial positions of a material element of fluid at times t and t', respectively. The relationship of r to r' is found through the kinematics, using

$$v'_r \equiv \frac{\partial r'}{\partial t'} = \frac{A'(t')}{r'^2} \tag{34}$$

Integration gives

$$\frac{1}{3} r'^3 = \int A' dt' + \frac{1}{3} C' = \frac{1}{3} R'^3 + \frac{1}{3} C'$$

or

$$r'^3(t') + C' \tag{35}$$

The constant of integration C' is found using the fact that $r' = r$ at $t' = t$. It follows that

$$r'^3 = r^3 + (R'^3 - R^3) \tag{36}$$

and

$$\underset{\sim}{\gamma}_{[o]} = \begin{pmatrix} 1 - \left(\frac{r'}{r}\right)^4 & 0 & 0 \\ 0 & 1 - \left(\frac{r}{r'}\right)^2 & 0 \\ 0 & 0 & 1 - \left(\frac{r}{r'}\right)^2 \end{pmatrix} \tag{37}$$

It follows further that the components of $\underset{\sim}{\gamma}_{[o]}$ may be written in terms of the bubble radius R upon noting that

$$\frac{r'}{r} = \left(1 + \frac{R'^3 - R^3}{r^3}\right)^{1/3} \tag{38}$$

It must be kept in mind that the components of $\underset{\sim}{\gamma}_{[o]}$ are functions of r, t', and t.

To find the history of the bubble collapse, $R(t)$, one must solve the Rayleigh equation, as derived in our previous studies[15] in the form

$$\rho\left(R\ddot{R} + \frac{3}{2}\dot{R}^2\right) = P_R - P_\infty + \int_R^\infty [\nabla \cdot \underset{\sim}{\tau}]_r \, dr \tag{39}$$

As in the previous work[15] we may reduce this to the form

$$P_G - P_\infty - 2\gamma/R - \rho\left(R\ddot{R} + \frac{3}{2}\dot{R}^2\right) = -2\int_R^\infty \frac{\tau_{rr} - \tau_{\theta\theta}}{r}\,dr \qquad (40)$$

where γ is the surface tension, and $P_G - P_\infty = -\Delta P$ is the pressure difference between the bubble interior and the liquid far from the bubble.

For the Newtonian liquid, for which

$$\underset{\sim}{\tau} = \mu \underset{\sim}{\Delta} \qquad (41)$$

we find $R(t)$ from the Rayleigh equation in the form

$$-\Delta P - 2\gamma/R - \rho\left(R\ddot{R} + \frac{3}{2}R^2\right) = 4\mu\,\dot{R}/R \qquad (42)$$

We may use Eq. 42 as an aid in experimental design, and we will return to this point shortly.

5. EXPERIMENTAL DESIGN

The design concept requires that a small gas bubble be created within the liquid of interest. An excess pressure upon the liquid will then cause the bubble to collapse. The history of collapse, $R(t)$, will reflect the properties of the liquid, and will be described by a solution to the Rayleigh equation, Eq. 40. This history will be recorded through high speed photography.

Prior to designing an experiment it is necessary to establish the working range of parameters that will be used. We wish to use the observation of bubble collapse to infer something about the rheology of the fluid

surrounding the bubble.

If the dynamics is too rapid, fluid inertia will control the bubble response, and mask the role of rheology. Thus, it is essential that the experiment be designed so as to minimize inertial effects. At the same time, the dynamics must be fast enough so that the high deformation rates typical of drop shattering are simulated. The result is that there is a narrow "operating window" of acceptable parameters.

We can use the Newtonian form of the Rayleigh equation to quantify some of these ideas.

We begin with the assumption that the collapse is so fast that it is adiabatic, and there is no time for diffusion of gas to occur. Hence there is a constraint between pressure and volume. Assuming an ideal gas we find

$$P_G V^m = \text{constant} \tag{43}$$

where P_G is an absolute pressure, and where m is the heat capacity ratio

$$m = C_p/C_v \tag{44}$$

A more useful form is

$$P_G R^{3m} = P_{oG} R_o^{3m} \tag{45}$$

where P_{oG} is the initial (absolute) pressure inside the bubble, upon initiation of collapse.

Hence

$$-\Delta P = P_G - P_\infty = P_{oG}\left(\frac{R_o}{R}\right)^{3m} - P_\infty$$

$$= P_{oG} - P_\infty + P_{oG}\left[\left(\frac{R_o}{R}\right)^{3m} - 1\right]$$

$$= -\Delta P_o + P_{oG}\left[\left(\frac{R_o}{R}\right)^{3m} - 1\right] \qquad (46)$$

The Rayleigh equation takes the form

$$-\Delta P_o + P_{oG}\left[\left(\frac{R_o}{R}\right)^{3m} - 1\right] - 2\gamma/R - \rho\left(R\ddot{R} + \frac{3}{2}\dot{R}^2\right) = 4\mu\dot{R}/R \qquad (47)$$

subject to initial conditions

$$R = R_o\,, \quad \dot{R} = 0 \qquad \text{at} \qquad t \leq 0$$

Note that for $t < 0$, the bubble is in equilibrium ($R = R_o$) at a pressure given by (setting $R = R_o$ and $\dot{R} = 0$ in Eq. 47)

$$-\Delta P_o - 2\gamma/R_o = 0$$

or

$$P_{oG} = P_\infty + 2\gamma/R_o \qquad t < 0 \qquad (48)$$

Collapse is initiated upon incrementing the external pressure by an amount P_1 so that

$$\Delta P_o = P_\infty - P_{oG} = P_1 - 2\gamma/R_o \tag{49}$$

Upon introducing Eqs. 48 and 49 into Eq. 47 we find

$$- P_1 + 2\gamma/R_o + \left(P_\infty + 2\gamma/R_o\right)\left[\left(\frac{R_o}{R}\right)^{3m} - 1\right] - 2\gamma/R$$

$$- \rho\left(R\ddot{R} + \frac{3}{2}\dot{R}^2\right) - 4\mu\dot{R}/R \tag{50}$$

We may first inquire into the total extent of collapse. For long time, when $\dot{R}$ approaches zero, we find from Eq. 50 that

$$- P_1 + 2\gamma/R_o + \left(P_\infty + 2\gamma/R_o\right)\left[\left(\frac{R_o}{R}\right)^{3m} - 1\right] - 2\gamma/R = 0 \tag{51}$$

For the sake of simple calculation, let us neglect surface tension in Eq. 51 and find

$$\frac{R_\infty}{R_o} = \left(1 + \frac{P_1}{P_\infty}\right)^{-1/3m} = \left(\frac{P_\infty + P_1}{P_\infty}\right)^{-1/3m} \tag{52}$$

where R_∞ is the final radius of the collapsed bubble. We see that the degree of collapse depends upon the ratio of absolute pressures before and after initiation of collapse.

If we take a reasonable value for the heat capacity ratio m to be m = 1.4 for diatomic gases we can prepare a simple table of collapse ratios as a function of pressure ratios.

Table. Collapse Ratios as a Function of Pressure Ratios (m = 1.4)

$\frac{P_\infty + P_1}{P_\infty}$	1	2	3	5	10	30	100
$\frac{R_\infty}{R_o}$	1	0.85	0.77	0.68	0.58	0.44	0.33

According to this estimate (which neglects surface tension) a pressure ratio in excess of ten is required to collapse the bubble by a factor of two. This is a sufficiently accurate estimate for the purpose of design of the experiment. We conclude that in order to achieve a reasonable degree of bubble collapse (in effect, enough data to be meaningful) we will have to use pressure ratios of order ten.

The next problem to deal with in experimental design is the rate of collapse, since this will determine the degree of need for high speed recording technology. Again, estimates are most easily made using Eq. 50 (i.e., assuming Newtonian behavior) and neglecting surface tension. A simple, but useful, analytical model follows if we neglect the gas pressure inside the

bubble. This provides an estimate for collapse that would be valid for short times, and small extents of collapse. Again, we note that the goal here is the development of simple guides to experimental design.

If we go back to the Rayleigh equation in the form of Eq. 42, and assume that ΔP is constant, neglect surface tension, and neglect inertial effects, we find

$$\frac{R}{R_o} = \exp\left(-\frac{\Delta P}{4\mu} t\right) \tag{53}$$

A useful time scale, from this model, is the time to collapse to $1/e = 0.37$ of the initial size. (Note that under constant pressure, ignoring the internal gas, the bubble collapses totally.)

This time scale is

$$t_e = 4\mu/\Delta P \tag{54}$$

For a 10 poise liquid collapsing under a 100 psi pressure difference, we find $t_e = 6 \times 10^{-6}$ s. This time scale is too short for existing technology. We note that liquids of interest could well be less viscous than 10 poise (further shortening the time scale). This result suggests that it will be necessary to collapse under small pressure differences. However, the previous result on extent of collapse indicates the need for large pressure ratios. It may be necessary to operate at sub-atmospheric pressure, so that $1 + P_l/P_\infty$

remains small. For example, if the system is initially at 0.5 psia (which requires a cold sample since the vapor pressure of water, for example, is not much less than this at room temperature) and is subjected to a 5 psia pressure, so that $\Delta P = 4.5$ psia while $P_1/P_\infty = 10$, then we might expect a measurable bubble collapse with a time scale of 10^{-4} s. It is clear that we will be dealing with very high speed events.

Another parameter that can be controlled is the bubble size R_o. If R_o is too large, inertial effects dominate the collapse. If this is the case, then rheological effects are unimportant, and it is not possible to extract rheological information from an experiment dominated by inertial forces.

Figure 3 shows solutions of the full Rayleigh equation for a Newtonian liquid for bubbles of initial radii of 50 and 100 micrometers. For the larger bubble, and the lower viscosity, some oscillation of the bubble occurs before it reaches its equilibrium final size. This is an inertial effect. For 10 and 100 poise liquids, the collapse is monotonic. Shown on Figure 3 is the purely viscous solution (Eq. 53), and we see that even the 10 poise liquid deviates from that model at small time, again demonstrating some degree of inertial resistance to collapse. However, the 100 poise liquid shows purely viscous collapse over most of its history.

By contrast, for a bubble of 50 micrometers radius, no oscillation occurs in the 5 poise liquid, and nearly viscous behavior is seen at 10 poise. It would appear from these simulations that it will be necessary to use bubbles of 50 micrometers radius or less in order to minimize inertial effects.

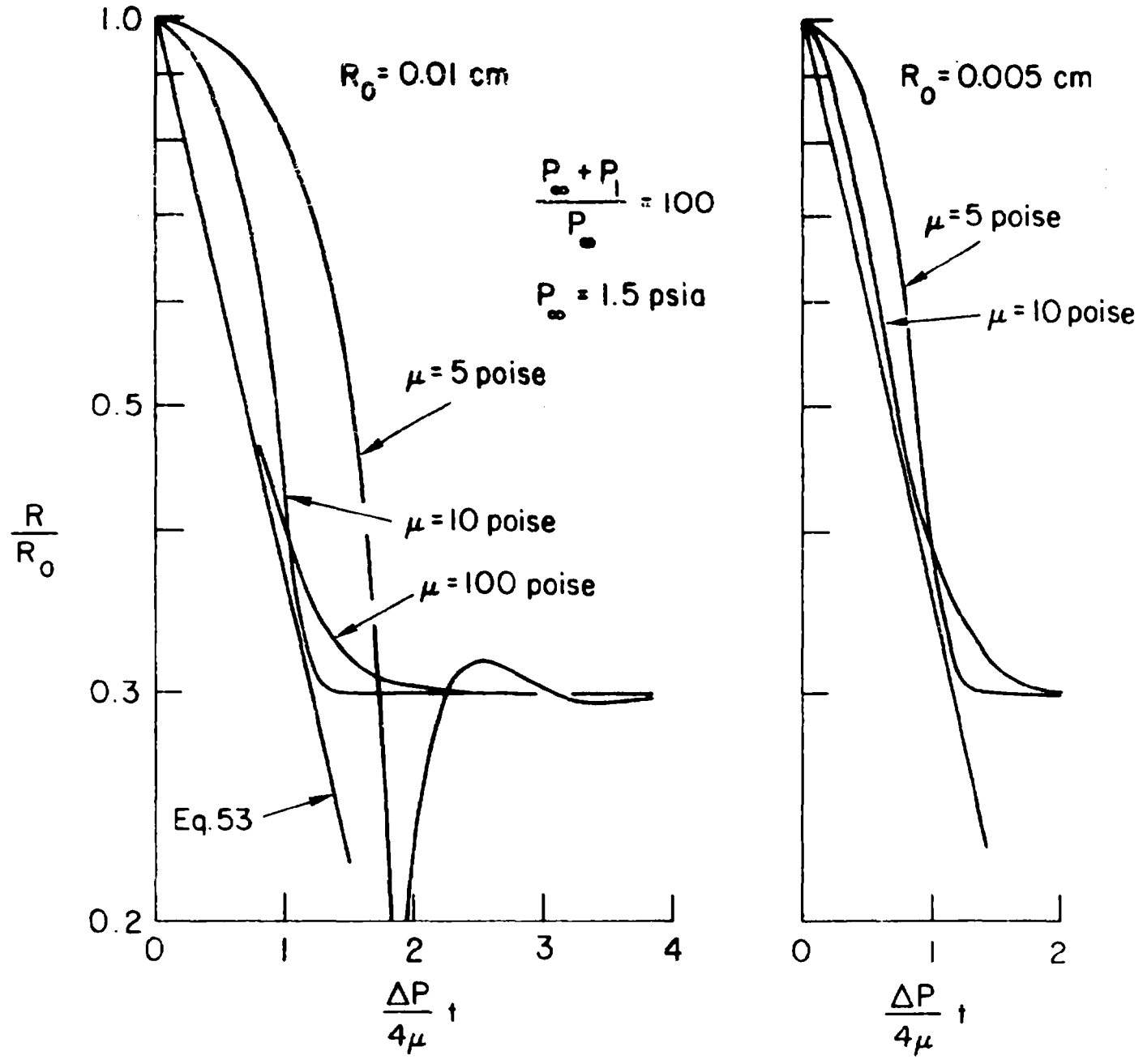
1.0
0.5
0.3
0.2
R/R0
R0 = 0.01 cm
(P∞ + P1)/P∞ = 100
P∞ = 1.5 psia
μ = 5 poise
μ = 10 poise
μ = 100 poise
Eq. 53
0
1
2
3
4
ΔP/4μ t
R0 = 0.005 cm
μ = 5 poise
μ = 10 poise
0
1
2
ΔP/4μ t

6. THE EXPERIMENTAL SYSTEM

6.1 Apparatus

A schematic of the experimental system is shown in figure 4, and a photograph of the actual apparatus is given in figure 5. The entire system was set up in a room which could be made completely dark, for photographic purposes. The experimental system may be conveniently separated into four distinct portions, which may be analyzed individually. The numbers in parentheses refer to the schematic in figure 4.

6.1.1 Cell:

The heart of the system is the glass/copper cell (1) with the platinum electrode mounted in it. Figures 6 and 7 are, respectively, a schematic and photograph of the cell. The glass is standard glass tubing with O.D. = 0.25", I.D. = 0.020" and L = 1.5". The copper is standard copper tubing with O.D. = 0.25", I.D. = 0.185" and L = 1.5". The glass and copper tubes are cemented together using Devcon® 5-minute epoxy. The acrylic supports are added to increase strength and provide a way to mount the cell onto the microscope stage.

Figure 8 is a schematic of the platinum electrode. The platinum wire (O.D. = 100 μm) is fused into the glass sleeve by melting the glass around the wire. The top of the electrode is then finely polished. The platinum electrode is mounted into the glass cell

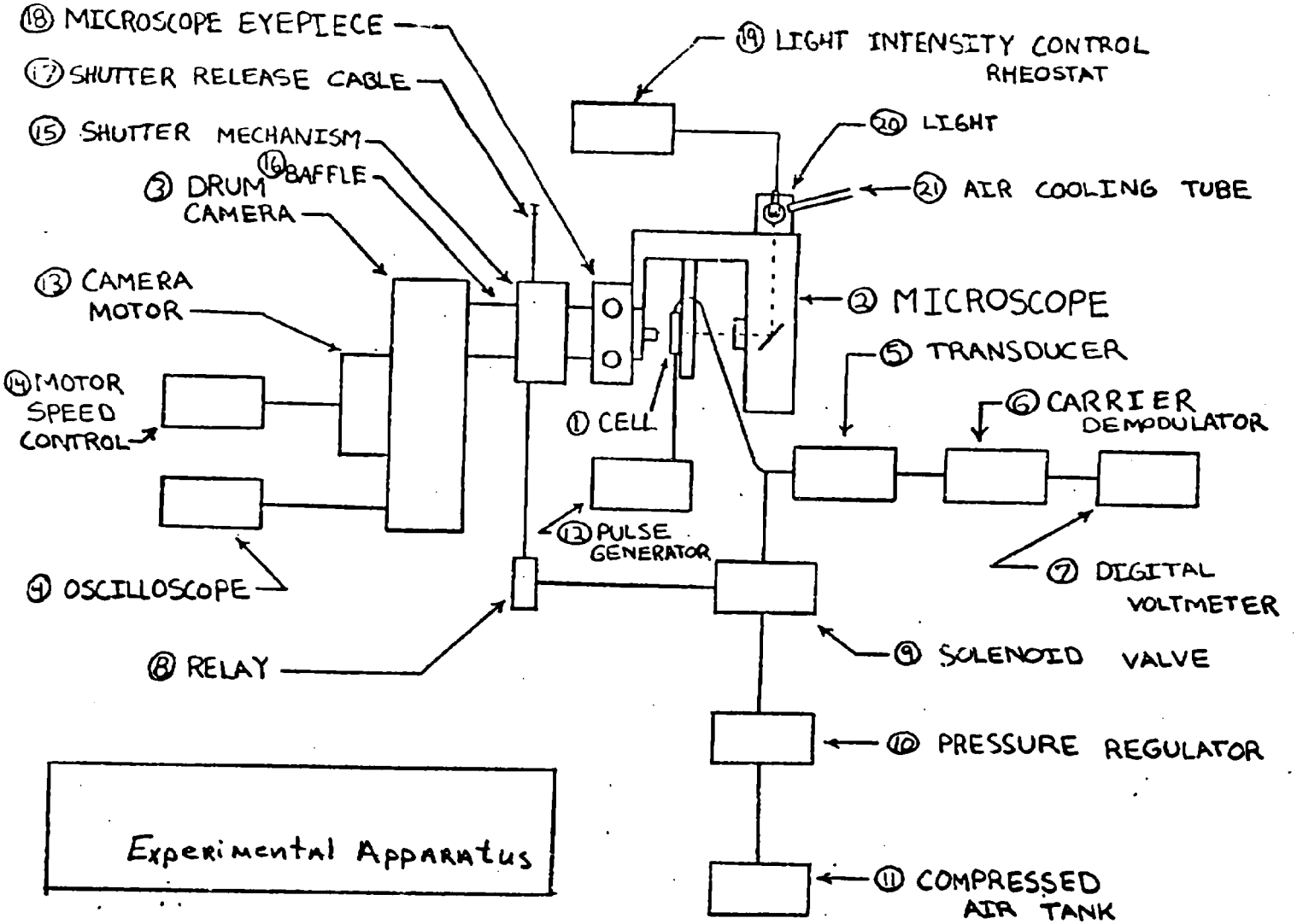

Experimental Apparatus

Figure 4

Figure 5

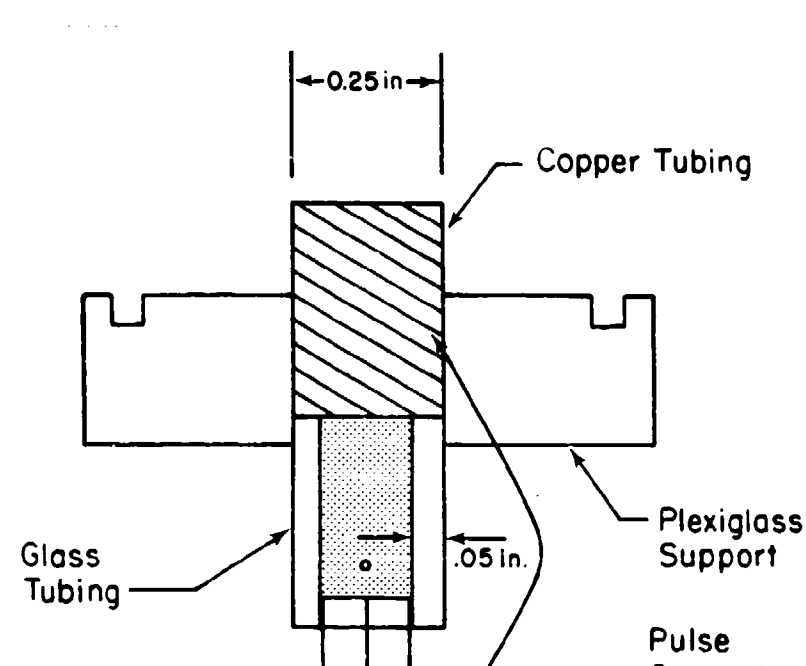

Glass Cell

Figure 6

Figure 1

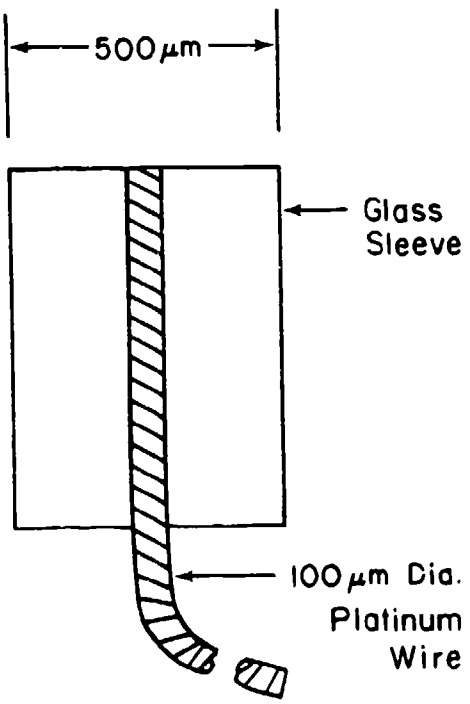

Platinum Wire Electrode

Figure 8

using a high temperature epoxy. Two leads come off the cell to the pulse generator (12), one from the platinum wire at the bottom of the cell and the other from the copper tubing at the top. When the glass/copper cell is filled with a conducting liquid (i.e., the test solution) the electric circuit is completed. Bubbles are generated using a Tektronix® 160A Power Supply, 161 Pulse Generator and 162 Waveform Generator in series (12). Bubbles of various sizes can be made by varying pulse width and magnitude. The electric pulse hydrolyzes the water and forms a hydrogen gas bubble which then rises in the liquid.

6.1.2 Optical System:

The optical system is a self-contained unit consisting of a Leitz® microscope (2, 18) with a Wild® MPS-11 Shutterpiece mechanism (15) attached. The microscope assembly is mounted in a horizontal position (as opposed to the usual vertical, stand-up position) on a wooden platform which can be raised and lowered. This allows for easy alignment with the rotary drum camera (3). The cell is fixed to the microscope stage, which moves left to right and forward/backward to allow centering and focusing of the rising gas bubble. The microscope optics were used as delivered, but the lighting system was modified for photographic purposes. The 12 V, 50 W Halogen-Bellaphot® (OSRAM) lamp

provided with the original system was replaced with a 120 V, 600 W tungsten-halogen (Sylvania) lamp (20). A Powerstat® adjustable transformer (19) was used to allow variable lighting control. It was also necessary to add an air cooling system (21) for the lamp. This extra lighting capability was one of the keys to obtaining streak photographs with reasonable contrast.

6.1.3 Photographic System:

A Beckman and Whitney Model 224 Rotary Drum Camera (3, 13) was used to do the high speed photography. A Variac® Type 100-Q adjustable transformer was used to provide motor speed control (14). In the rotary drum camera filming speed is not determined by framing rate but is instead a function of rotation speed. A continuous length of film is wound along the drum of the camera and the drum is then rotated at a known speed. A continuous streak photograph is then obtained. The rotation speed is measured by taking an electronic signal which comes from the back of the camera and feeding this into a Tektronix® T912 storage oscilloscope (4), from which the number of revolutions per second of the camera drum can be determined. Therefore, for this system a number analogous to framing rate is given as mm film/sec.

The Wild® MPS-11 Shutterpiece (15) was used to control exposure times. This uses an electronic shutter mechanism so this signal was also used to trigger the solenoid valve in the pressure system. Variable shutter speeds are available but 1/15 sec proved to be a convenient speed at which to conduct the experiments. A black cardboard baffle (16) was made to connect the shutter mechanism to the lens of the rotary drum camera. This prevented extraneous light from entering into the lens. The lens of the drum camera was completely covered except for a vertical slit approximately 1/16" wide. This collimated light source was essential to obtaining good contrast on the streak photographs. Kodak 2475 Recording film (1000 ASA) was found to provide the best balance of high speed and good contrast.

6.1.4 Pressure System:

To collapse the bubble, which is at atmospheric pressure in the cell, it was necessary to pressurize the system. The source of the pressure was a compressed air cylinder (11) controlled by a Purox® CGA-580 pressure regulator (10). To instantaneously pressurize the system a fast acting valve was needed. A Schroder Bellows® cyclone three-way direct acting solenoid valve (9) was chosen. (Schroder Part # 74323-0115, Orifice 1/16/1/16, 120V/60 Hz, brass body.) The solenoid valve was activated by an

electronic trigger from the MPS-11 Shutterpiece via an electronic relay (GE #SC-43/530T) (8). In this way synchronization of the pressure pulse and shutter opening was made possible. There was a short time delay between shutter opening and pressurization of the system so it was certain that the event would not occur before the shutter had opened. Pressure was measured using a Validyne® DP15 variable reluctance differential pressure transducer (5) in conjunction with a Validyne® CD15 sine wave carrier demodulator (6), connected to a digital voltmeter (Hewlett-Packard) (7). Various pressure plates (diaphragms) are available for the transducer, so that a wide pressure range can be covered. The pressure hose was connected directly to the top of the cell (copper section) using a hose clamp and some RTV® Silicone rubber sealant. The cell was able to withstand pressures up to 160 psig.

6.2 Experimental Procedure.

The fluid to be used is loaded into the cell using a disposable pipet. Care must be taken to make sure that the fluid level is beyond the glass/copper interface, because contact with the copper is necessary to complete the circuit for the bubble hydrolysis. The pressure tubing is then fastened to the top of the cell, using both a hose clamp and RTV Silicone Rubber sealant (GE). The entire assembly is mounted onto the moveable stage of the microscope. The leads from the pulse generator are attached to the cell; one to the platinum

wire which extends out the bottom of the cell and the other to the copper tubing on top.

Next, the room is made completely dark and the film is loaded into the drum camera. Each experimental run uses one 35 mm roll (36 exposure) of the Kodak 2475 recording film. The drum camera is equipped with a three position lever (shut, focus, and open), so that after the film is loaded the lever is moved to the shut position and the lights in the experimental system can be put on. The drum camera is set in motion and its speed monitored using the Tektronix® storage oscilloscope. A shutter speed of 1/15 sec is chosen for the experiment so the drum speed must be kept below 15 rev/sec. Typically, experiments are run at 8 to 12 rev/sec (125 to 80 m sec/rev). The significance of this time with respect to the streak photographs will be explained later.

Next, the pulse generator and pressure system are turned on. Various size bubbles in the range of 50 to 500 μm can be made, depending on pulse width and magnitude. In general, for the purpose of photographic simplicity, bubbles in the 200 to 300 μm range are used. Once made, the bubble rises slowly up the cell until it comes into viewing range. (Note: In the fluids that were studied in these experiments, it was found that the upward movement of the bubble is much "slower" than the time scale of the experiment, so for all practical purposes the bubble is treated as stationary.

For less viscous fluids, such as pure water for instance, this can be a big problem.) At this point the lever on the camera is moved to the focus position, and the bubble can be aligned and focused while one looks through the viewing port at the back of the drum camera. The moveable microscope stage makes it easy to center and focus the drop. With everything in position the shutter is closed and set to 1/15 sec, the lever on the camera is put in the open position and the pressure on the air tank regulator is set to the desired level (typically 60 to 160 psig). Now, the shutter is opened, which triggers the solenoid valve through the electronic relay, and opens the cell to the desired pressure. The bubble collapses and the event is recorded on film in the form of a "streak photograph" (which will be discussed later). The rotation speed of the drum camera is obtained from the storage scope and the pressure is read from a calibrated digital voltmeter attached to the sine wave demodulator.

Once again, the room is made completely dark and the film is removed from the drum camera, loaded onto a 35 mm developing reel and placed in a standard light-tight developing tank. The film is "push-processed" by developing for 11 to 12 min. in Kodak DK-50 developer (recommended developing time is 5 to 6 min.). The end result is a streak photograph of the bubble collapse, as is shown in figure 9.

6.3 Solutions.

The solutions that were used in this study were all water soluble polymer systems. The two polymers used were carboxymethylcellulose (CMC)

Figure 7

(Hercules, Inc. CMC 7H3S, experimental sample) and polyacrylamide (PAA) (Stein, Hall and Co., Polyhall 295). The four solutions that were used in this study are CMC 1%: PAA 0.25, 1.0 and 1.5% where X% is defined as wt. polymer/wt. H_2O.

The rheological properties of these samples were obtained using a Rheometrics® Fluids Rheometer in the cone and plate geometry and the dynamic oscillatory mode. Figure 10 shows the complex viscosity (η^*) for the four samples. In the limit of $\omega \to 0$, $\eta^* \to \eta_o$, the steady state zero-shear viscosity, and over the entire frequency range the behavior of η^* parallels that of η. From the plots of complex viscosity versus frequency several characteristics of the fluids are apparent. First, in every case the PAA solutions are more highly non-newtonian than the CMC solution. Second, below ω = 10 rad/sec, the CMC solution behaves essentially as a Newtonian fluid. Hence, we hope to be able to use this CMC solution as a psuedo-newtonian fluid for experimental purposes.

The dynamic storage (elastic) and loss (viscous) moduli, G' and G'' respectively, for the four solutions are given in figure 11. Once again, there is a marked difference in the behavior of the CMC and PAA solutions. In the case of CMC, the viscous forces (G'') are always substantially greater than the elastic forces (G'). For the PAA solutions at the low frequencies, the viscous forces (G'') are larger than the elastic forces (G'), but as the frequency gets higher the two forces become equal in magnitude and finally the elastic forces begin to dominate. This markedly different behavior between the PAA and CMC might allow one to speculate

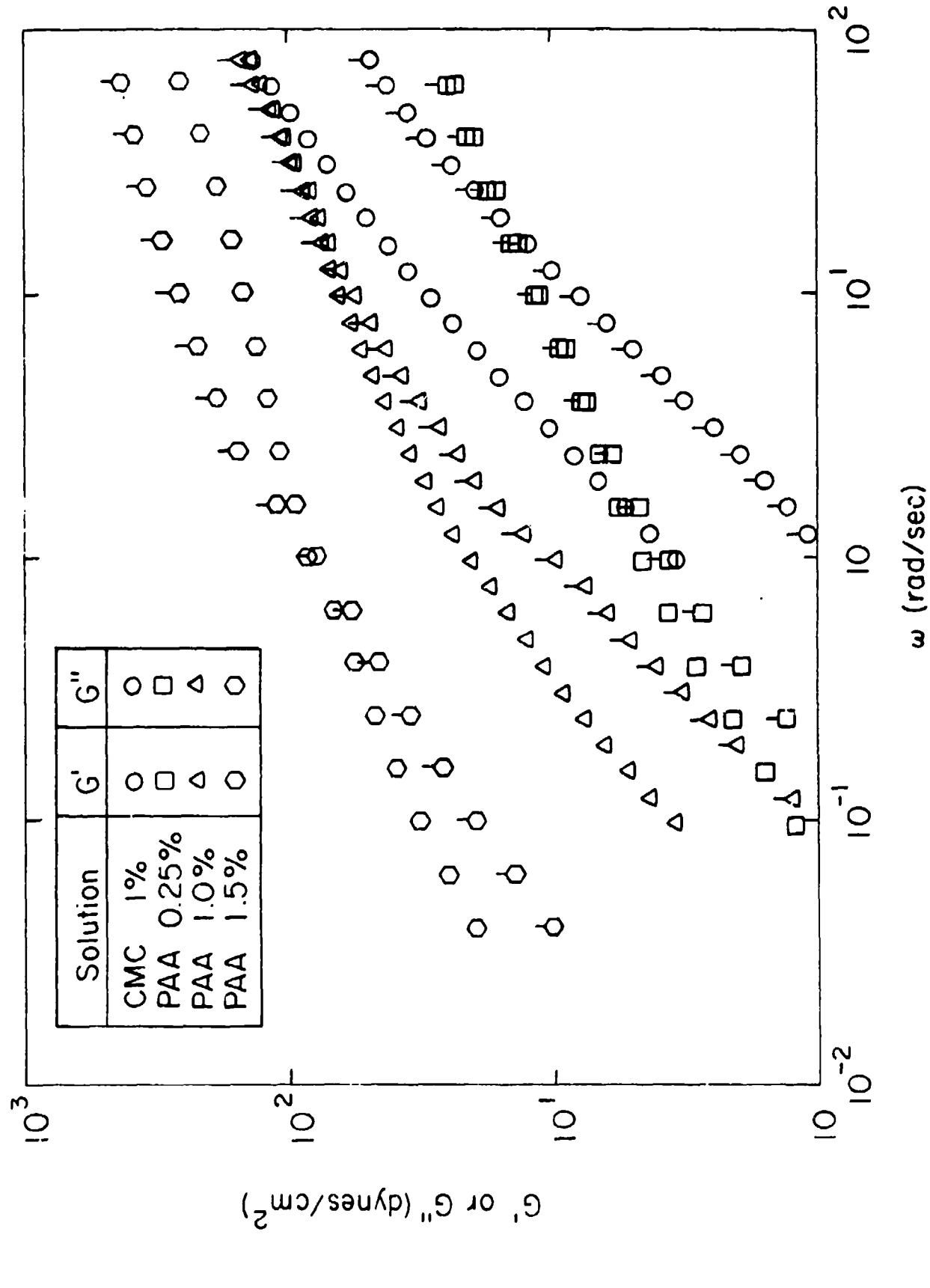

Figure 10

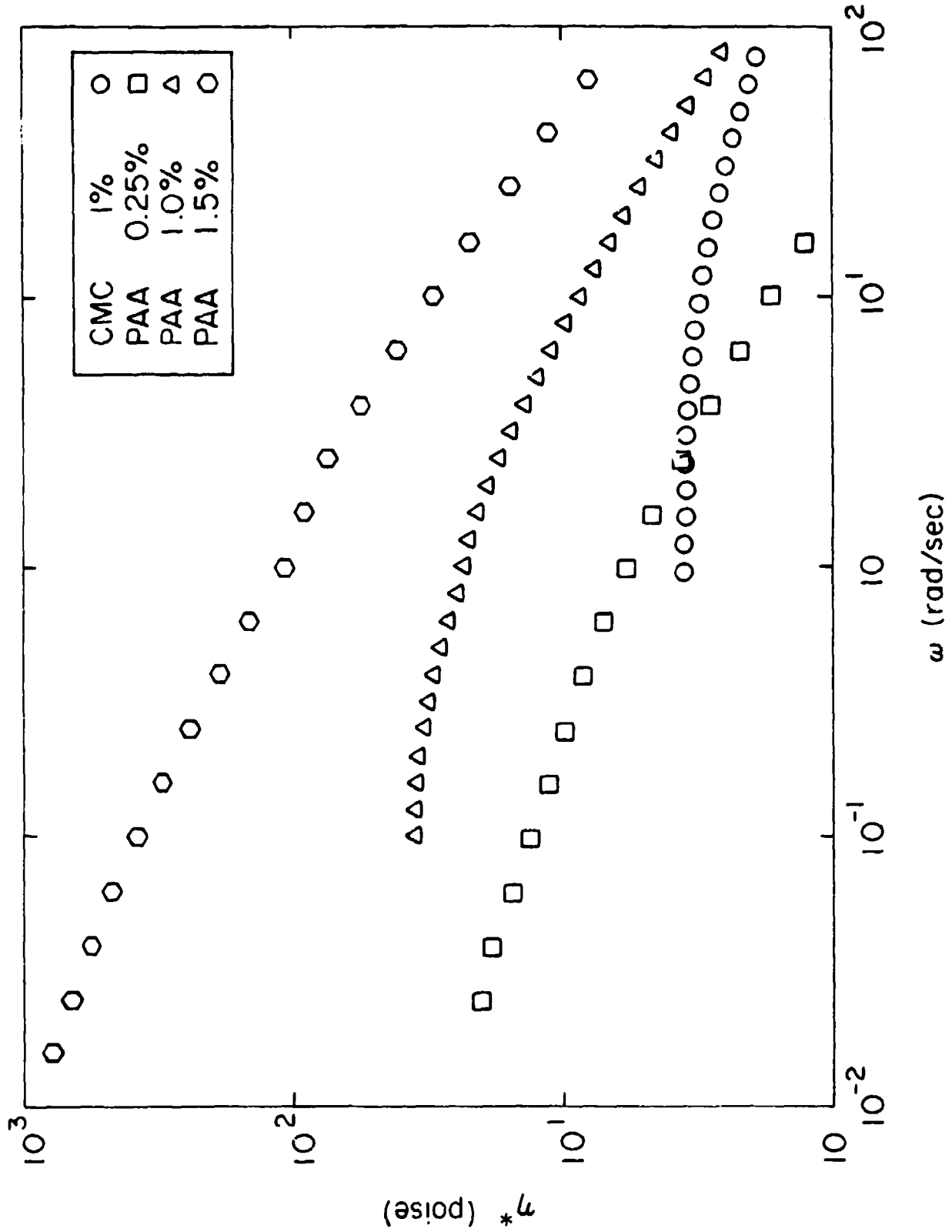
CMC 1%
PAA 0.25%
PAA 1.0%
PAA 1.5%
10^3
10^2
10^1
10
10^{-2}
10^{-1}
10^1
10^2
η^* (poise)
ω (rad/sec)

Figure 11

that the elastic forces would be a factor in one case and not in the other. It is also evident that the frequency (strain rate) range of the experiment could be very important in determining fluid behavior because of the strong frequency dependent nature of the polymer solutions.

7. CALIBRATION AND ANALYSIS OF EXPERIMENTAL DATA

7.1 Magnification Calibration.

To determine the total magnification in the optical system a simple test was conducted. A thin chromel wire (O.D. = 0.0093") was inserted into the cell when it was filled with a test fluid. A series of still photographs were taken with the rotary drum camera. From the wire dimensions measured on film and the known (measured) diameter of the wire, a magnification factor was determined. The magnification was found to be 55X.

7.2 Determination of Collapse Times.

Since there is no readily available time measure (such as framing rate) in the rotary drum camera, a method to calculate the time scale of the event had to be devised. What was done was to measure the perimeter of the drum where the film is placed during the experiment. This gives a measure of length per revolution. From the storage scope, the rotational speed is obtained. Thus, one is able to calculate length per second. Typical time scales for collapse were approximately 10^{-3} to 10^{-4} sec. From the streak photographs it is possible to calculate the "lag time" between the shutter opening and the pressure pulse hitting the fluid. This was found to

be approximately 15 msecs.

8. EXPERIMENTAL DATA

Figure 12 is a photograph of a single bubble taken with the rotary drum camera when it is not rotating and the slit has been removed from the camera lens. This bubble is approximately 200 μm in diameter. The white line in the center of the bubble is caused by the diffraction of light as it passes through the bubble.

If one starts with the bubble as pictured in figure 12 and covers the lens with a very narrow vertical slit, all that can be seen is a slice through the bubble. Therefore, with the camera rotating, the collapse appears as a streak of continually decreasing width. This is shown by the "streak photograph" given in figure 9. Referring to that photograph, one sees that there is an initial portion, which is indicative of the time between the shutter opening and the pressure pulse hitting the system. Once the pressure hits, the collapse begins (small oscillations can be seen initially) and the streak continues to decrease in width until the equilibrium bubble size is reached. The pressure remains constant throughout the run.

Analysis of the data consists of measuring the initial streak width and the width as a function of distance until no more change is observed. The streak width is correlated to the bubble diameter (using the magnification factor previously determined) and the distance along the film related to the time of collapse (using the rotation speed and length of film per rotation).

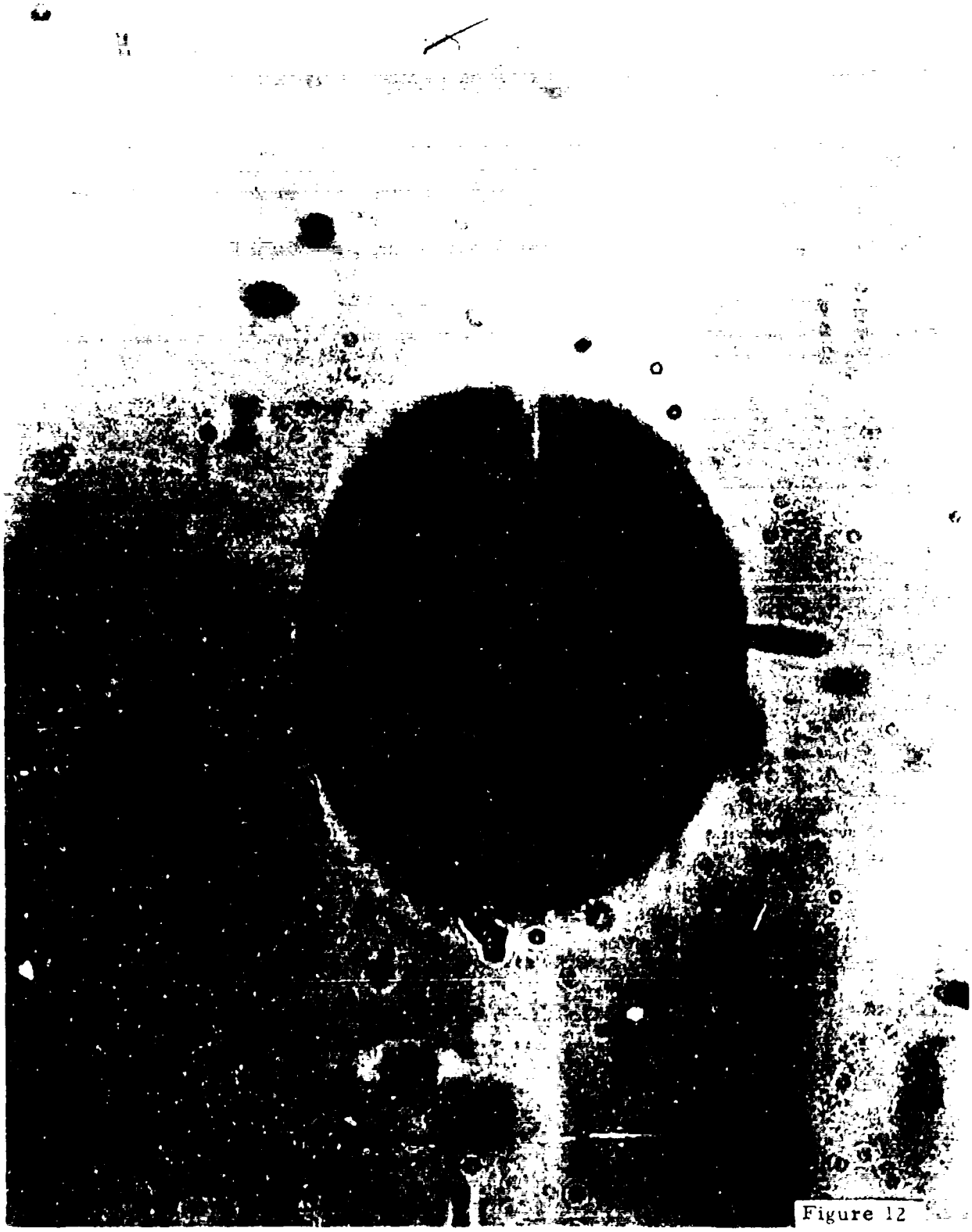

Figure 12

Figure 13 shows data from two bubble collapse runs — one for the relatively inelastic CMC solution and one for the more elastic PAA solution. The most striking observation is the similarity of collapse of the two fluids. Not obvious from the figure is the fact that the collapse is much slower than would be expected for these fluids. Finally we note that the collapse proceeds to a level below that predicted by Eq. 52, based on the adiabatic assumption. Similar results are observed in all cases studied to date. Additional data are in the appendix.

These results provide clues to problems in the experimental system that must be corrected.

9. EVALUATION AND DISCUSSION OF DATA

Let us begin with the positive accomplishments, and then examine the problems that remain.

We have designed, constructed, and tested a system for high speed photography of bubble collapse. While improvements in the photographic system are possible, it is clear that accurate and reliable data are possible. The prototype test cell is not made of glass of any optical quality. Additional experience with lighting and focusing techniques will lead to some improvement in the contrast and sharpness of the streak image. It should be possible to reduce the bubble size by factors of two to three and still obtain reliable data.

	R_0	P_∞	Run	Symbol
CMC 1%	105 μm	160 psig	# 17	○
PAA 0.25%	110 μm	160 psig	# 15	△

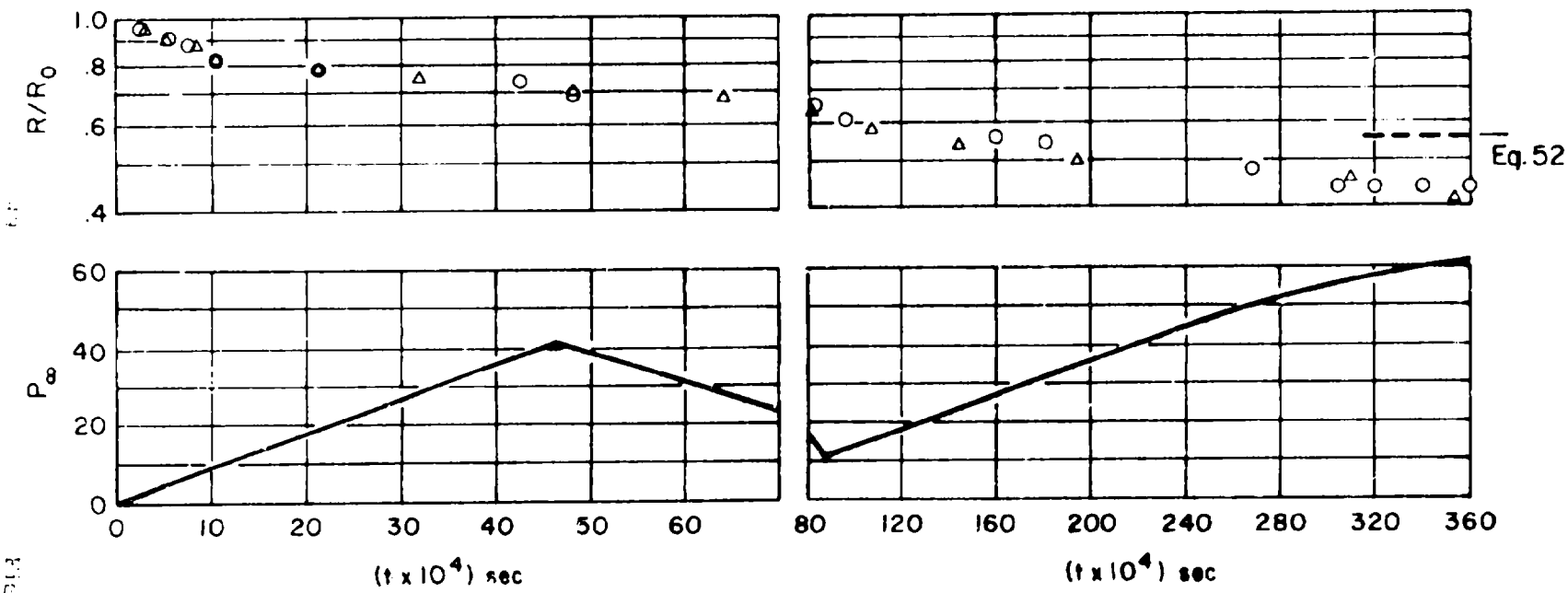

Figure 13

The technique for production of bubbles in aqueous solutions works well. In these preliminary tests relatively large bubbles have been used, of about 100 μm radius. It is not difficult to reduce the bubble radius to 30 to 50 μm, and we will note subsequently that this may be necessary.

The major problem lies in the imposition of a step-change in pressure upon the test cell. Superimposed upon figure 13 is a trace of the pressure measured in the test cell. It would appear that upon opening the solenoid valve there is a relatively rapid "spike" of pressure followed by a slow rise. Thus, the bubble is not collapsing under an instantaneous step-change to the new pressure. To date, it has not been possible to determine if the problem lies in the solenoid valve itself, or in some other feature of the design of the test cell/valve/pressure reservoir system. This would appear to be the major problem to be dealt with at this point in the development of the experimental system. Until this problem is solved, data obtained to date cannot be compared to any theoretical model based upon solution of the appropriate form of the Rayleigh equation.

10. RECOMMENDATIONS

10.1 There are several areas where improvements could be made in the experimental system to extend its usefulness and accuracy.

10.1.1 Cell.

A new cell could be made of higher quality glass. Special optical glass cells, as are used in spectrophotometers, are available commercially. It might be useful to make the cell rectangular in order to prevent any optical distortion that may occur when photographing through a circular cell.

10.1.2 Optical System.

It appears that most of the photographic problems which were encountered earlier in the project have been resolved. We would like to obtain sharper photographs, but a new cell should help considerably in this area. The keys to obtaining high contrast photographs are the very high intensity light and the use of the slit on the camera lens to exclude stray light.

10.1.3 Pressure System.

This is the area where the biggest improvements could be made. The solenoid valve used in our experiments is, to our knowledge, the fastest opening valve available for this pressure range. Unless some

improvement in this area of technolgy exists, of which we are unaware, it would appear that a solenoid valve will not be suitable for use with low viscosity fluids whose collapse times are of the order examined in our studies. The current technology is suited to "slower" fluids, i.e., more viscous fluids, or to collapse under smaller driving pressures (see 10.2.3 below).

An alternative to a solenoid valve should be explored. One possibility would be to separate the test cell and the pressure reservoir by a thin membrane or septum that could be punctured with a mechanical device. This alternative was not examined, and at this point we are unable to estimate the character of the pressure pulse that such a system would produce.

We conclude that the limitations of current technology for creating a change in pressure make it impossible to impose a suitable approximation to a "step change" in pressure on the bubble. However, the pressure pulse can be measured, and the theoretical analysis for bubble collapse could be suitably modified to account for the observed pressure pulse.

10.2 In addition to these hardware improvements, several changes in procedure would lead to more meaningful results.

10.2.1 Bubble Size.

Large bubbles have been used in these preliminary tests in

order to minimize photographic problems. A reduction by a factor of two to three, down to the range of 35 to 50 μm radius, is possible with the current design, and will ensure the elimination of inertial effects.

10.2.2 Bubbles in Non-Aqueous Solutions.

At the present time the bubble production system can only be used for aqueous materials. To extend the use of the system to organic materials, another means of bubble formation, not based on hydrolysis, is necessary.

A new technique for making small bubbles, suitable for both aqueous and organic solvents, has been discovered. Some of the solution of interest is placed in a high speed blender and beaten into a froth. A sample of this aerated liquid is removed. Most of the bubbles, because of their size, will rise and leave the liquid. High speed agitation of a viscous liquid will create some bubbles of extremely small size. The desired range is 50 to 100 microns diameter. These small bubbles will remain in the sample. With a hypodermic, a very small volume of the sample is removed. The volume is such as to contain only a few small bubbles. This sample is then introduced into the bottom of the test cell which contains the quiescent test liquid. When one of the small bubbles rises into the main body of the test liquid, the collapse experiment is initiated. Specific work remains to establish an optimum procedure with respect to agitation, sample size, etc. A modified test cell will have to be designed.

10.2.3 Reduced Pressures.

Ultimately one will wish to study more dilute, lower viscosity, solutions. In order to slow down the collapse, it will be necessary to use smaller driving pressures. However, it is still necessary to use large pressure ratios in order to achieve significant changes in bubble size. This will necessitate the use of sub-atmospheric pressure prior to collapse, followed by imposition of a small increment of pressure. For example, absolute pressures before and during collapse could be 0.5 psia and 5 psia. In this way the required large pressure ratio of order ten is maintained, while the pressure difference is only 4.5 psi. One possible advantage of this is the likelihood that it will be easier to produce an "instantaneous" step-change in pressure at lower pressure differences.

Of course, the lower limit on pressure is the vapor pressure of the solution. However, one could work with a cold solution, and extrapolate results to (higher) temperatures of interest through the use of classical time-temperature superposition principles.[11]

LITERATURE CITED

1. Adelberg, M. Mean Drop Size Resulting from the Injection of a Liquid Jet into a High-Speed Gas Stream. AIAA J. 6, 1143 (1968).

2. Wilcox, J. D., R. K. June, H. A. Brown, Jr., and R. C. Kelly, Jr. The Retardation of Drop Breakup in High Velocity Airstreams by Polymeric Modifiers. J. Appl. Polymer. Sci. 5, 1 (1961).

3. Wang, K-H., and C. Tien. Atomization and Drop Size of Polymer Solution. IEC Proc. Des. Dev. 11, 169 (1972).

4. Gerber, B. V., and A. K. Stuempfle. TSD 004.7-11. AD-A025999/4GA. A New Experimental Technique for Studying the Explosive Comminution of Liquids. Available from NTIS U. S. Dept. Commerce. 1976 Army Science Conference Proceedings. Vol. I. 1976 UNCLASSIFIED Report.

5. Simpkins, P. G., and E. L. Bales. Water-Drop Response to Sudden Accelerations. J. Fluid Mech. 55, 629 (1972).

6. Fishburn, B. D. Boundary Layer Stripping of Liquid Drops Fragmented by Taylor Instability. Acta Astron. 1, 1267 (1974).

7. Hanson, A. R., E. G. Domich, and H. S. Adams. Shock-Tube Investigation of the Breakup of Drops by Air Blasts. Phys. Fluids. 6, 1070 (1963).

8. Haas, F. C. Stability of Droplets Suddenly Exposed to a High Velocity Gas Stream. A. I. Ch. E. Journal. 10, 920 (1964).

9. Harper, E. Y., G. W. Grube, and I-D. Chang. On the Breakup of Accelerating Liquid Drops. J. Fluid Mech. 52, 565 (1972).

10. Ranger, A. A., and J. A. Nicholls. Aerodynamic Shattering of Liquid Drops. AIAA Journal. 7, 285 (1969).

11. Bird, R. B., R. C. Armstrong, and O. Hassager. Dynamics of Polymeric Liquids. Vols. 1 and 2. Wiley, NY. 1977.

12. Shirodkar, P., and S. Middleman. Lubrication Flows in Viscoelastic Liquids: I. Squeezing Flow between Approaching Parallel Rigid Planes. J. Rheology. 26, xx (1982).

13. Pearson, G. H. and S. Middleman. Elongational Flow Behavior of Viscoelastic Liquids: Part I. Modeling of Bubble Collapse. AIChE Journal. 23, 714 (1977).

14. Pearson, G. H. and S. Middleman. Elongational Flow Behavior of Viscoelastic Liquids: Part II. Definition and Measurement of Apparent Elongational Viscosity. AIChE Journal. 23, 722 (1977).

15. Pearson, G. H. and S. Middleman. Elongational Flow Behavior of Viscoelastic Liquids: Modeling Bubble Dynamics with Viscoelastic Constitutive Equations. Rheol. Acta. 17, 500 (1978).

APPENDIX

Experimental data on bubble collapse

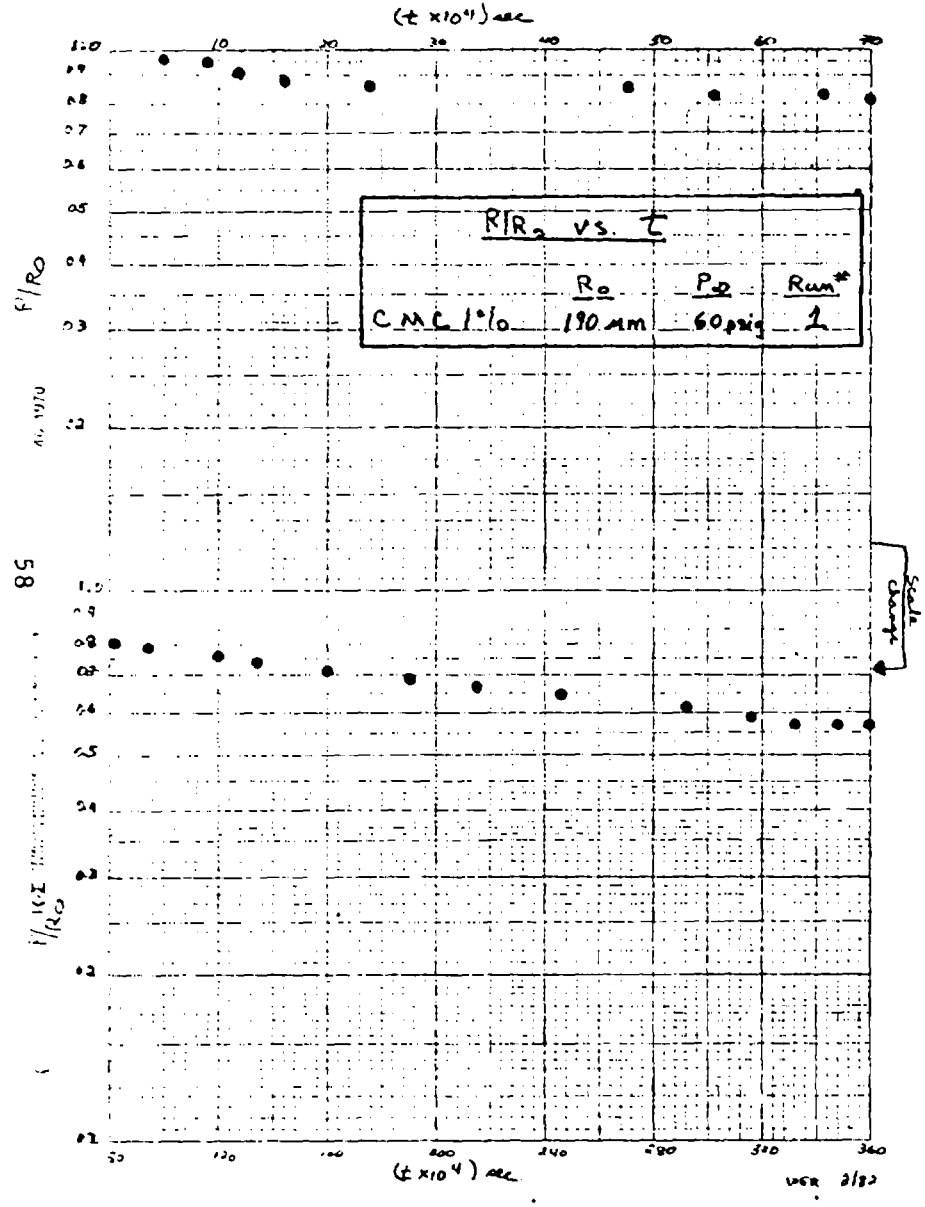
(t x10⁴) sec
R/Ro vs. t
Ro
Po
Run#
CMC 1%
190 mm
60 psig
1
R/Ro
scale change
(t x10⁴) sec

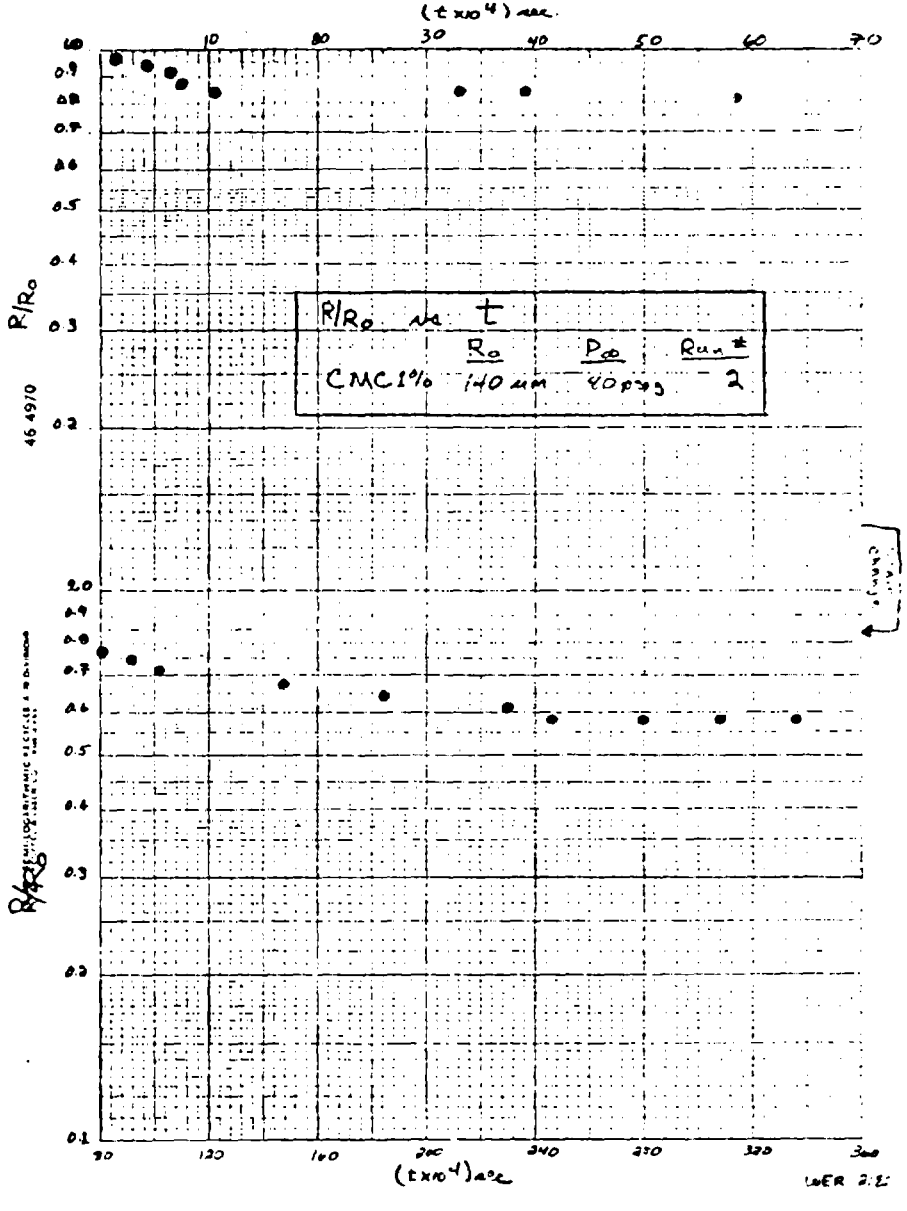
(t x10⁴) sec
R/Ro vs t
Ro
Po
Run#
CMC 1%
140 mm
40 psig
2
R/Ro
scale change
(t x10⁴) sec

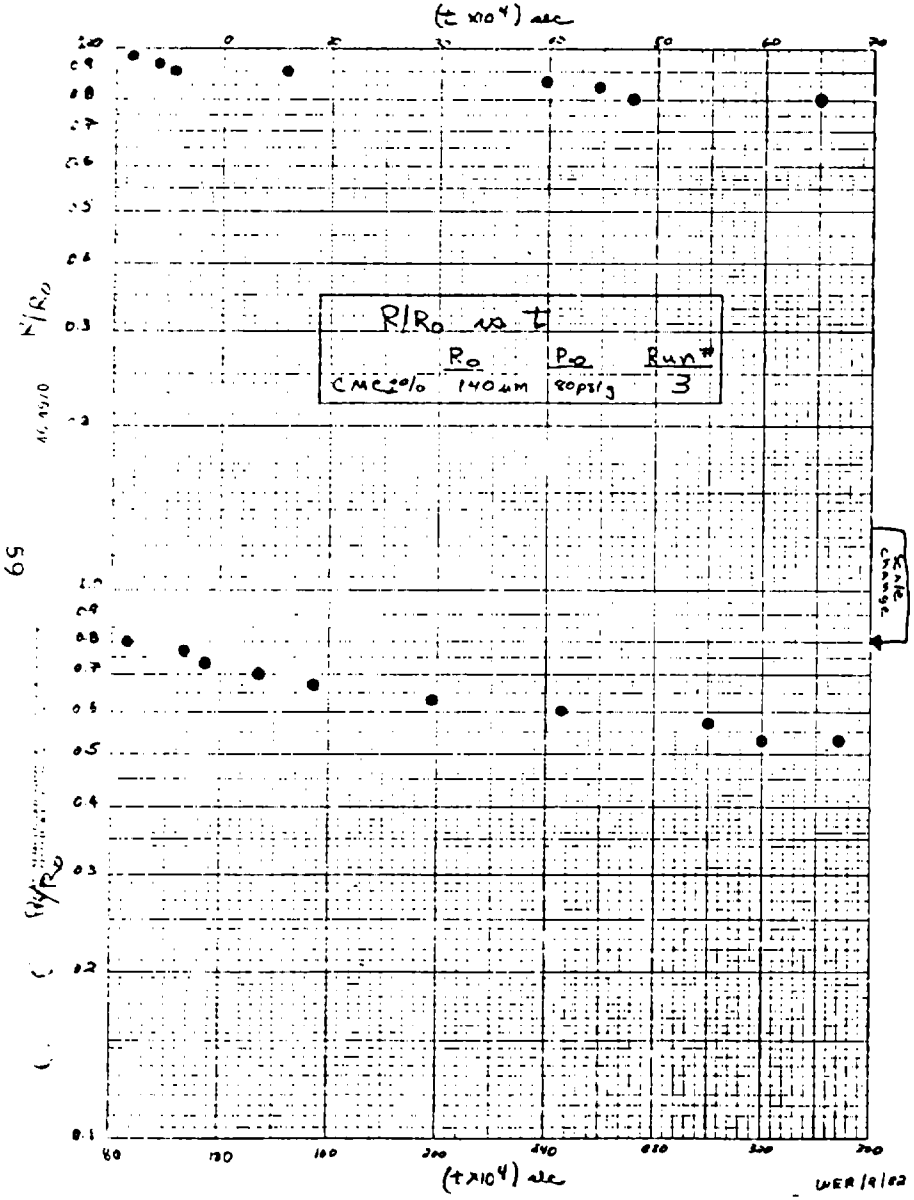
(t x10⁴) sec
R/Ro
R/Ro vs t
Ro
Po
Run#
CMC 2% 140 μm 80 psig 3
SCALE CHANGE
(t x10⁴) sec
WER 9/82

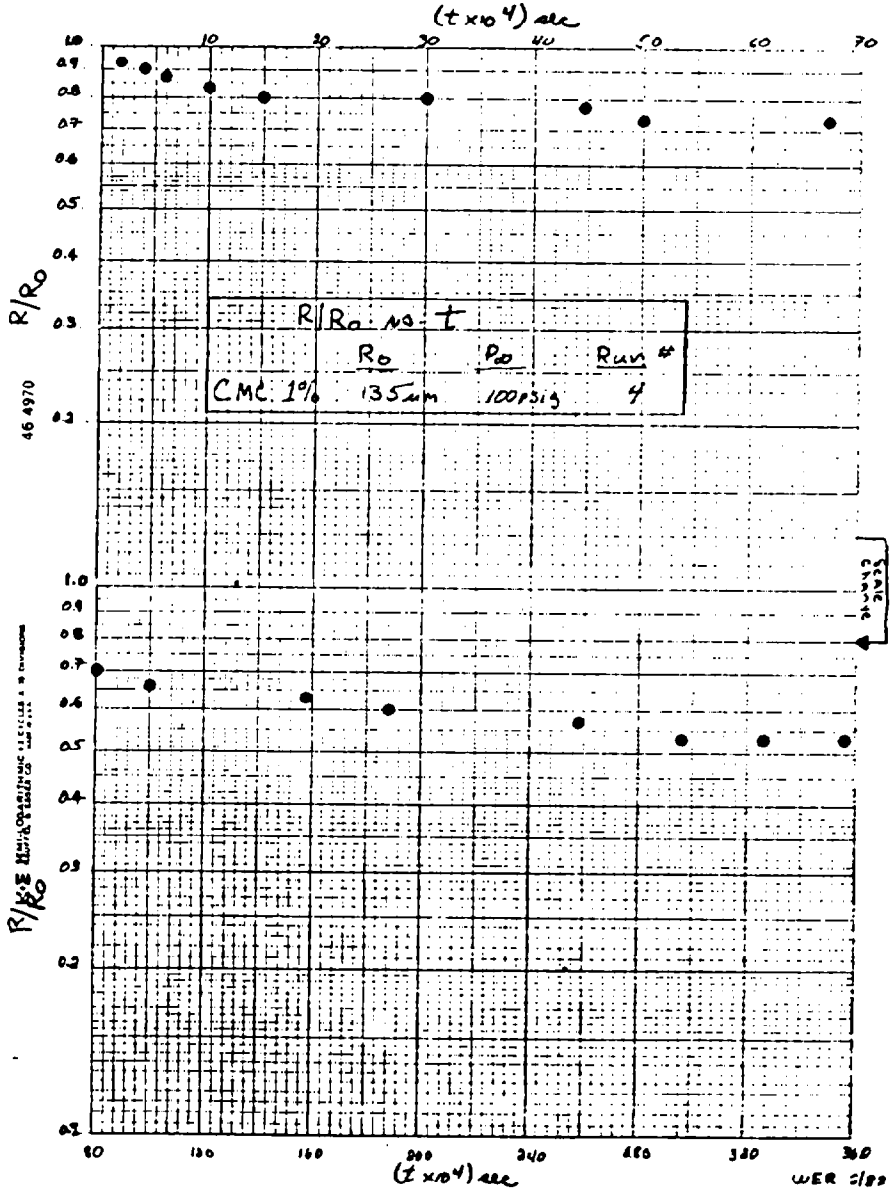
(t x10⁴) sec
R/Ro
R/Ro vs t
Ro
Po
Run #
CMC 1% 135 μm 100 psig 4
SCALE CHANGE
(t x10⁴) sec
WER 1/83

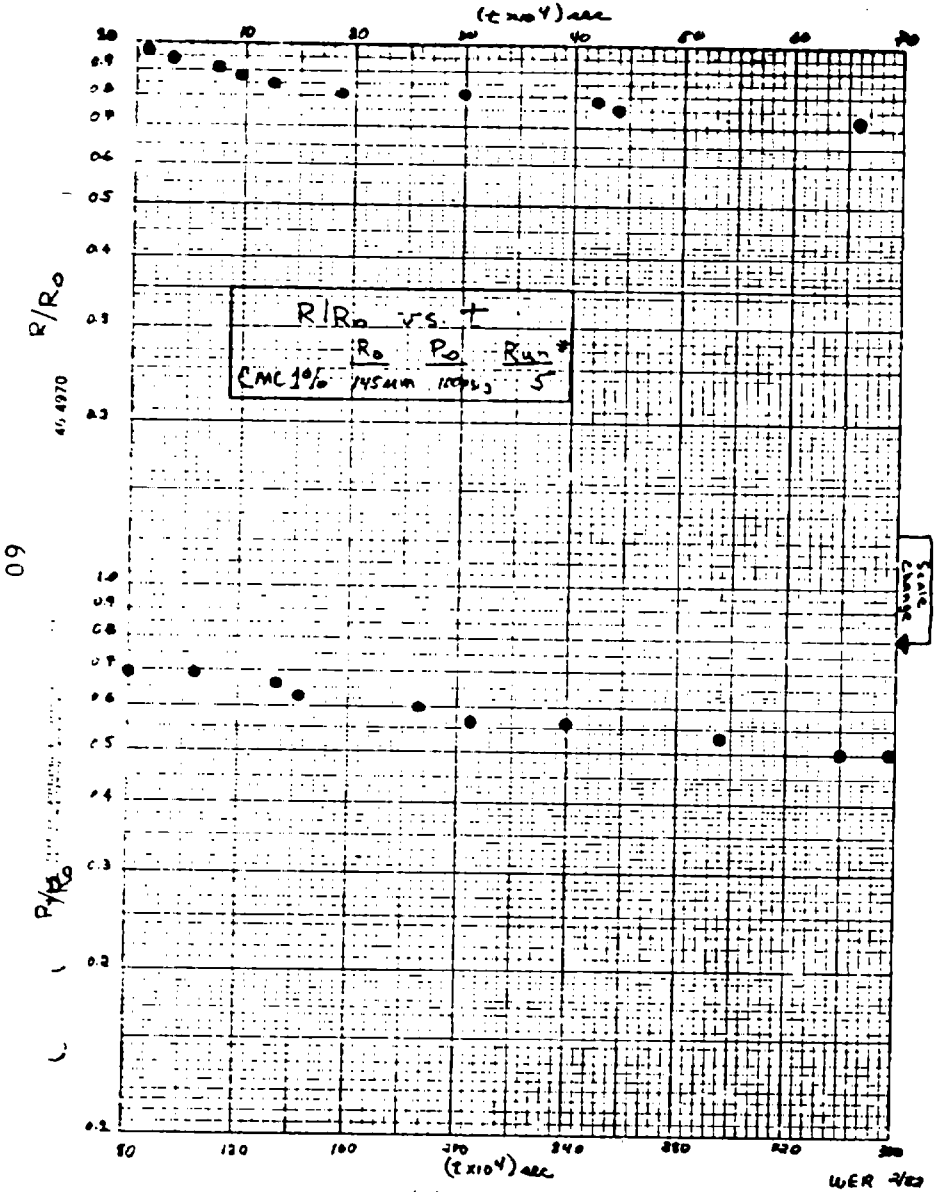
(t x10⁴) sec
R/R₀
R/R₀ vs t
Ro Po Run#
CMC 1% 145 mm 100 psig 5
(t x10⁴) sec
WER 2/82

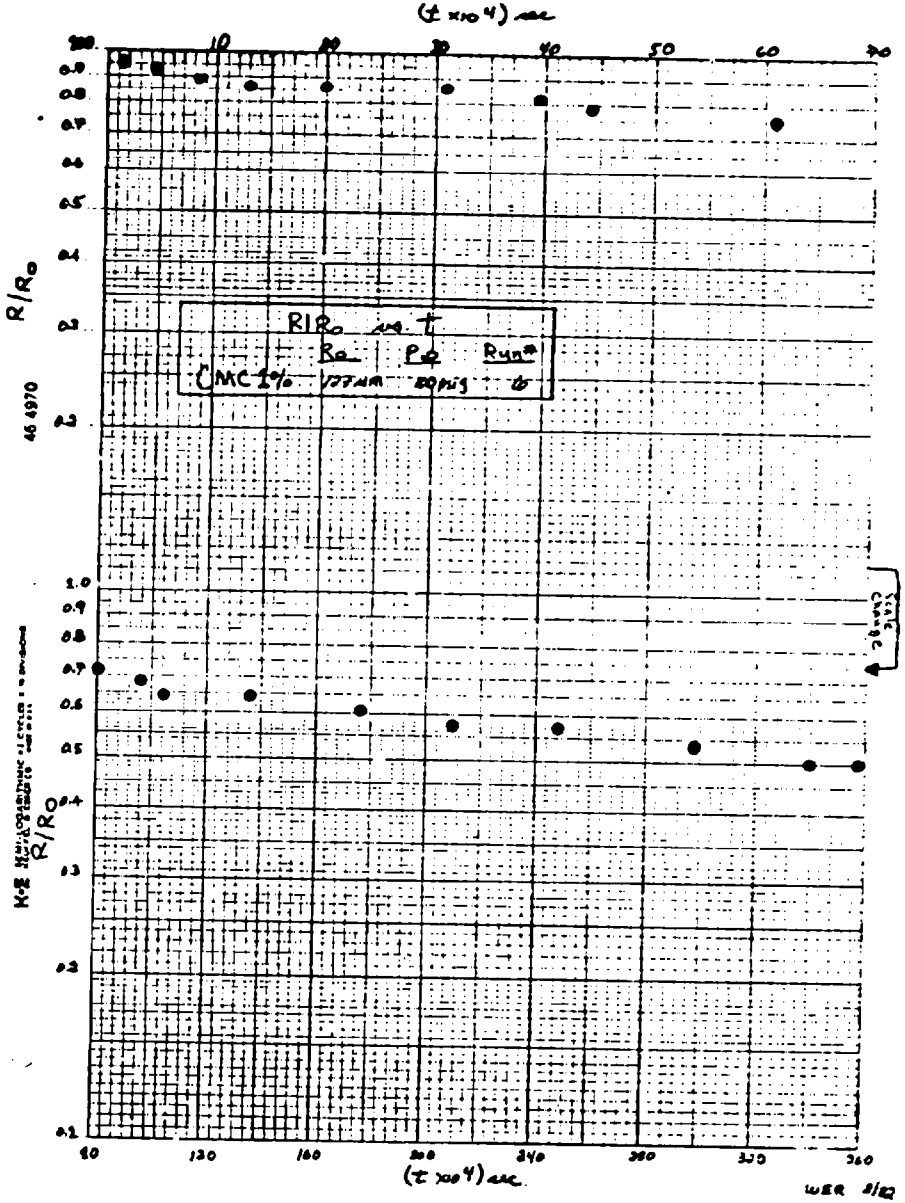
(t x10⁴) sec
R/R₀
R/R₀ vs t
Ro Po Run#
CMC 1% 177 mm 80 psig 6
(t x10⁴) sec
WER 2/82

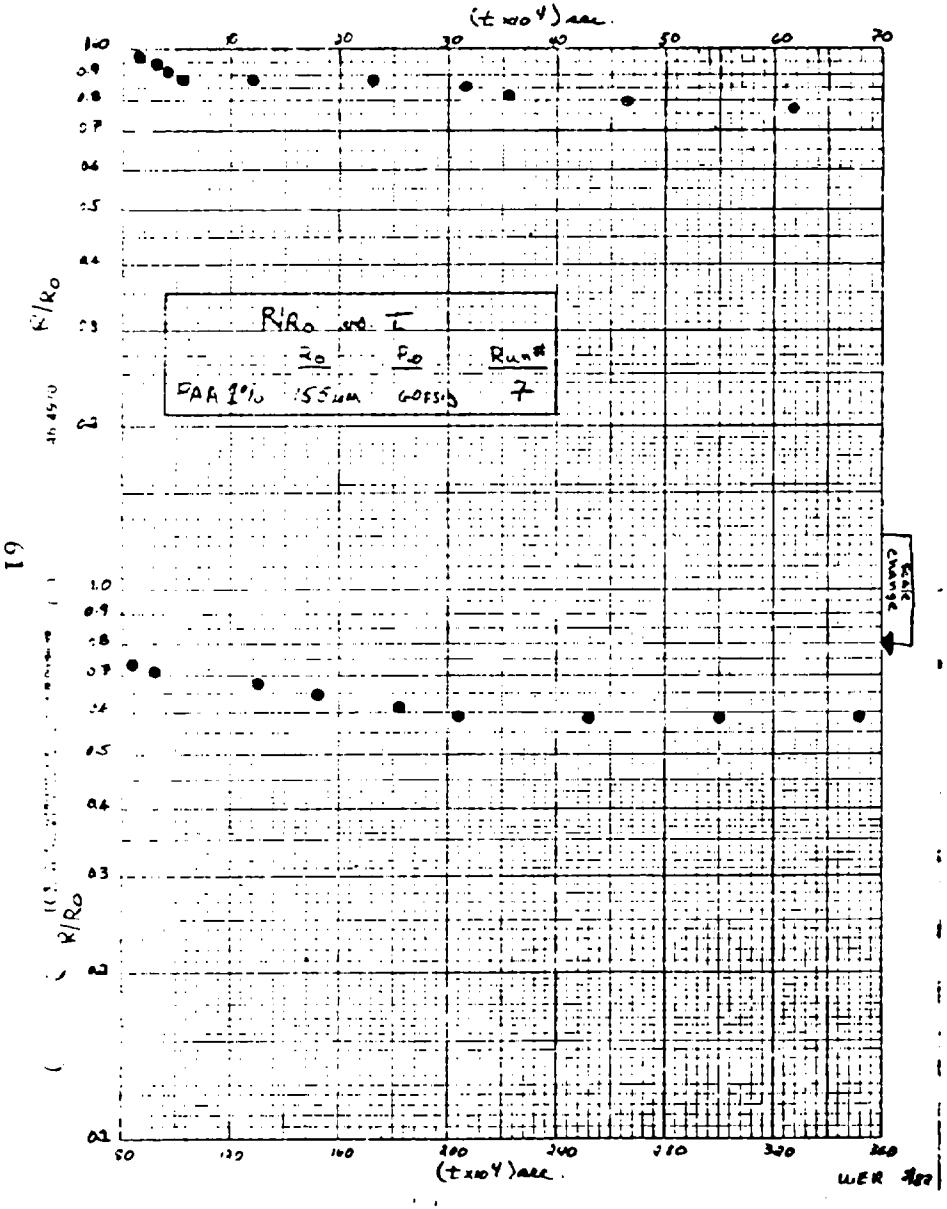
(t x10⁴) sec.
R/Ro vs t
Ro
Po
Run#
PAA 1%
155 μm
60 psig
7
R/Ro
Scale change
(t x10⁴) sec.

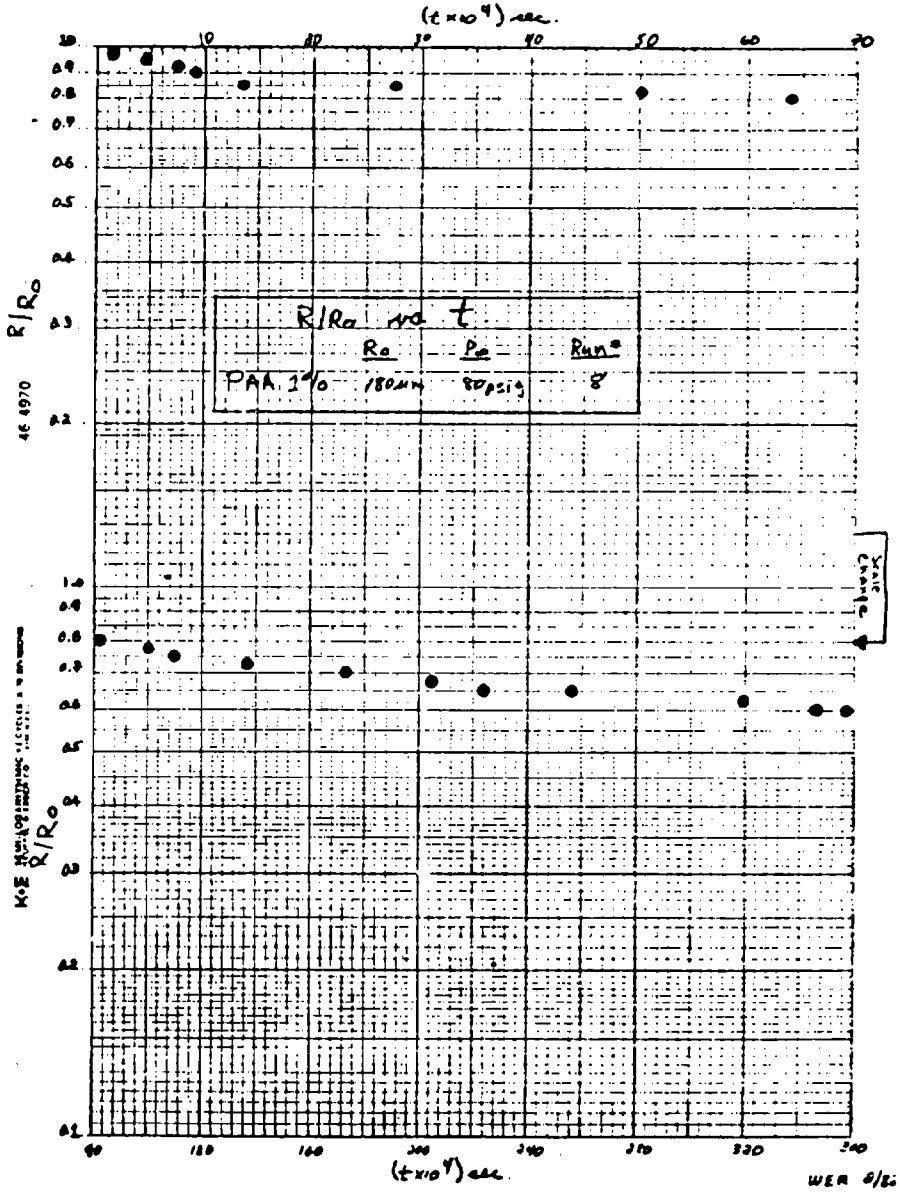
(t x10⁴) sec.
R/Ro vs t
Ro
Po
Run#
PAA 1%
180 μm
80 psig
8
R/Ro
Scale change
(t x10⁴) sec.

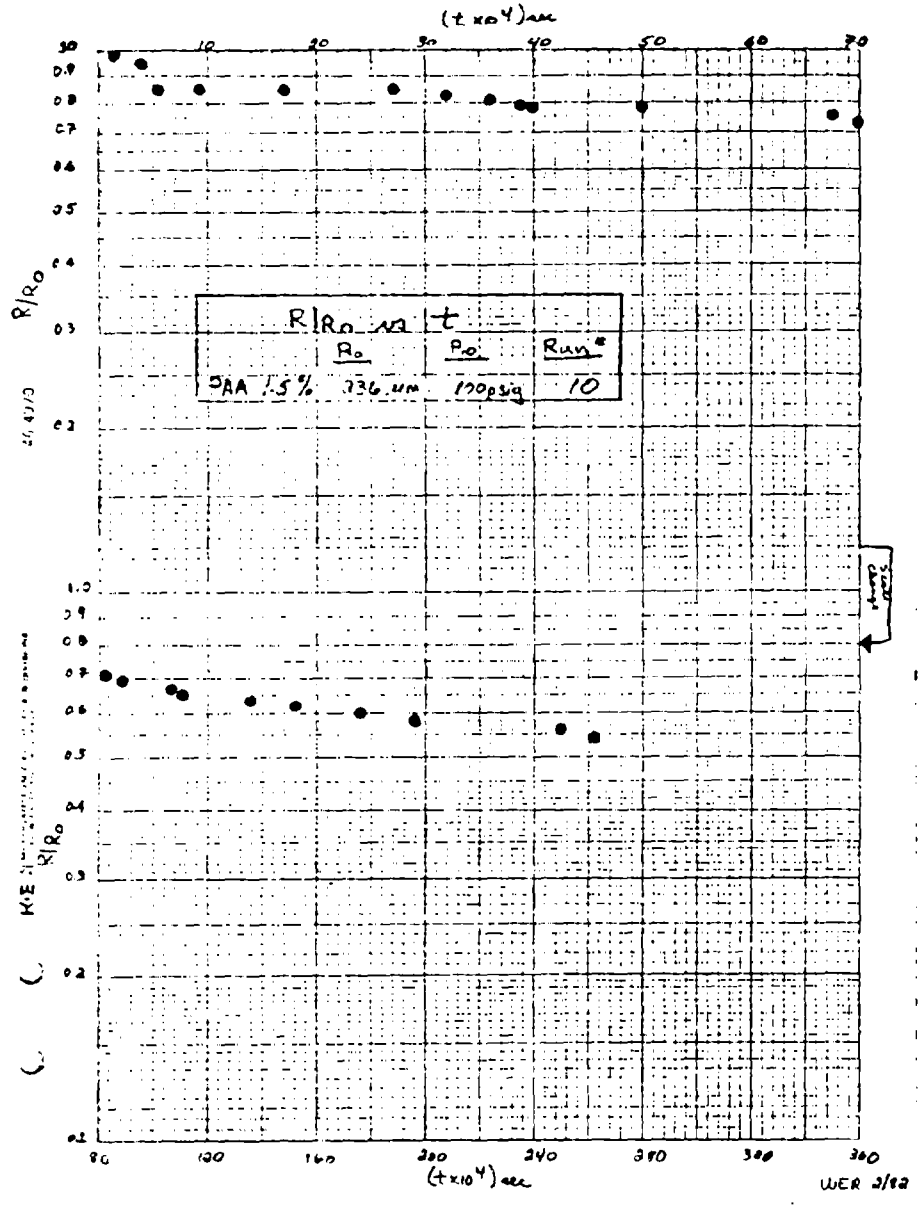
(t x10⁴) sec
R/Ro
R/Ro vs t
PAA 1.5%
Ro 736 um
Po 120psig
Run# 10
(t x10⁴) sec
WER 3/82

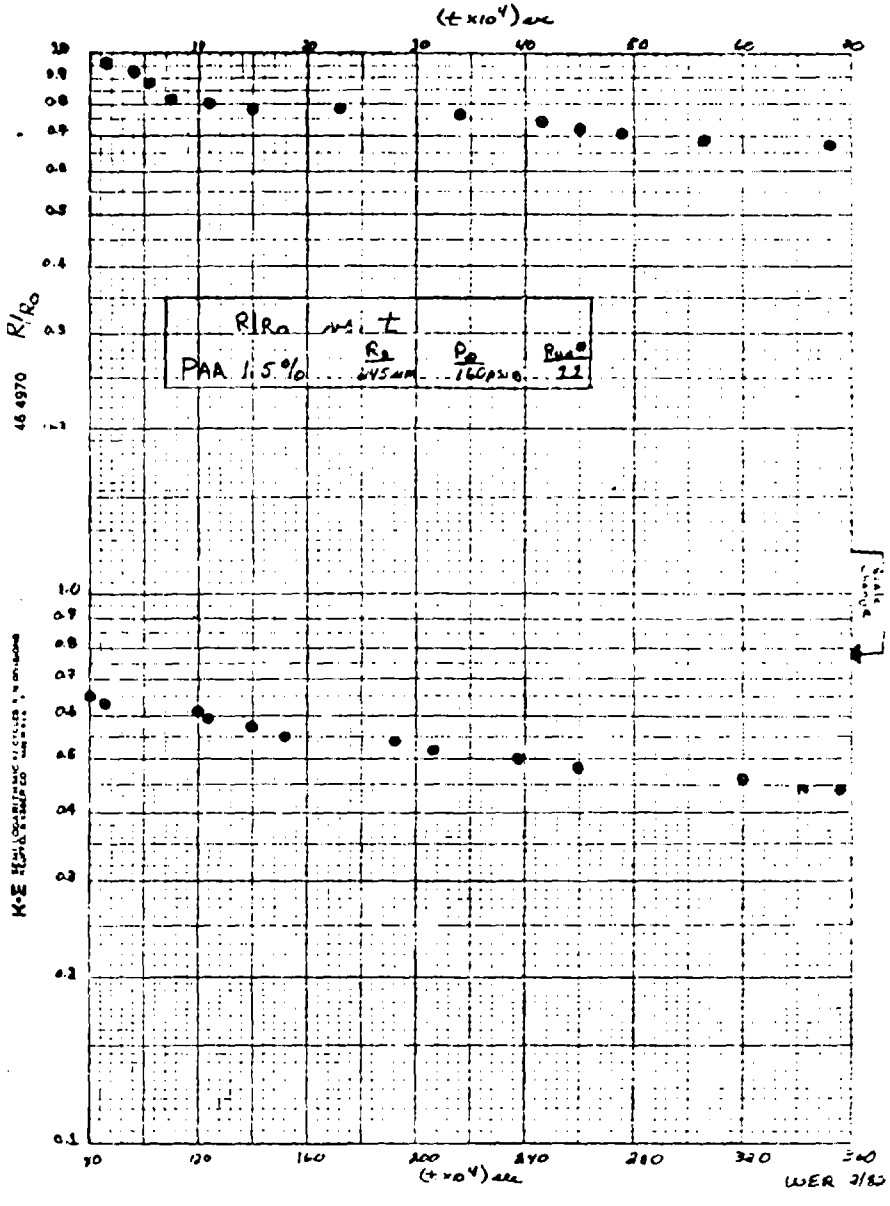
(t x10⁴) sec
R/Ro
R/Ro vs t
PAA 1.5%
Ro 645 um
Po 160psig
Run# 22
(t x10⁴) sec
WER 3/82

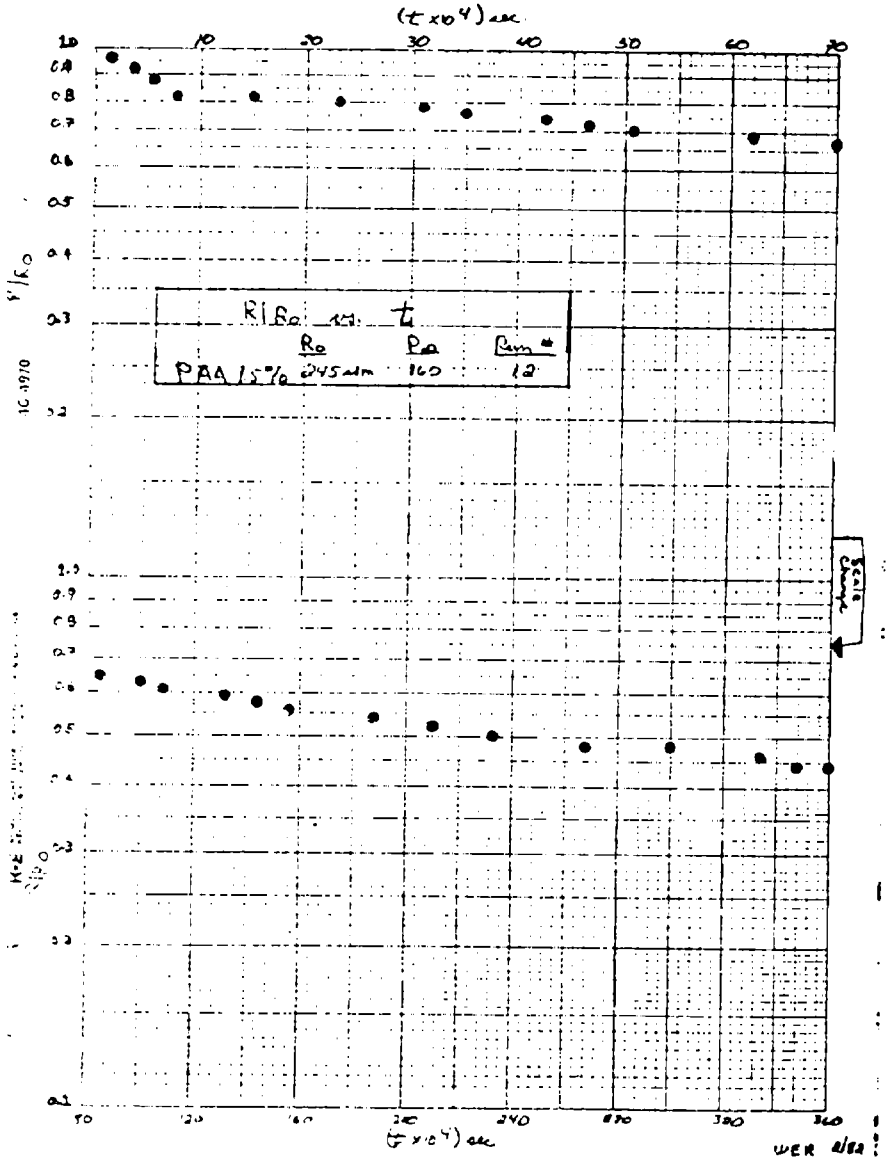
(t x10⁴) sec
R/Ro vs. t
Ro
Pa
Run #
PAA 1.5% 245 nm 160 12
R/Ro
Scale Change
(t x10⁴) sec

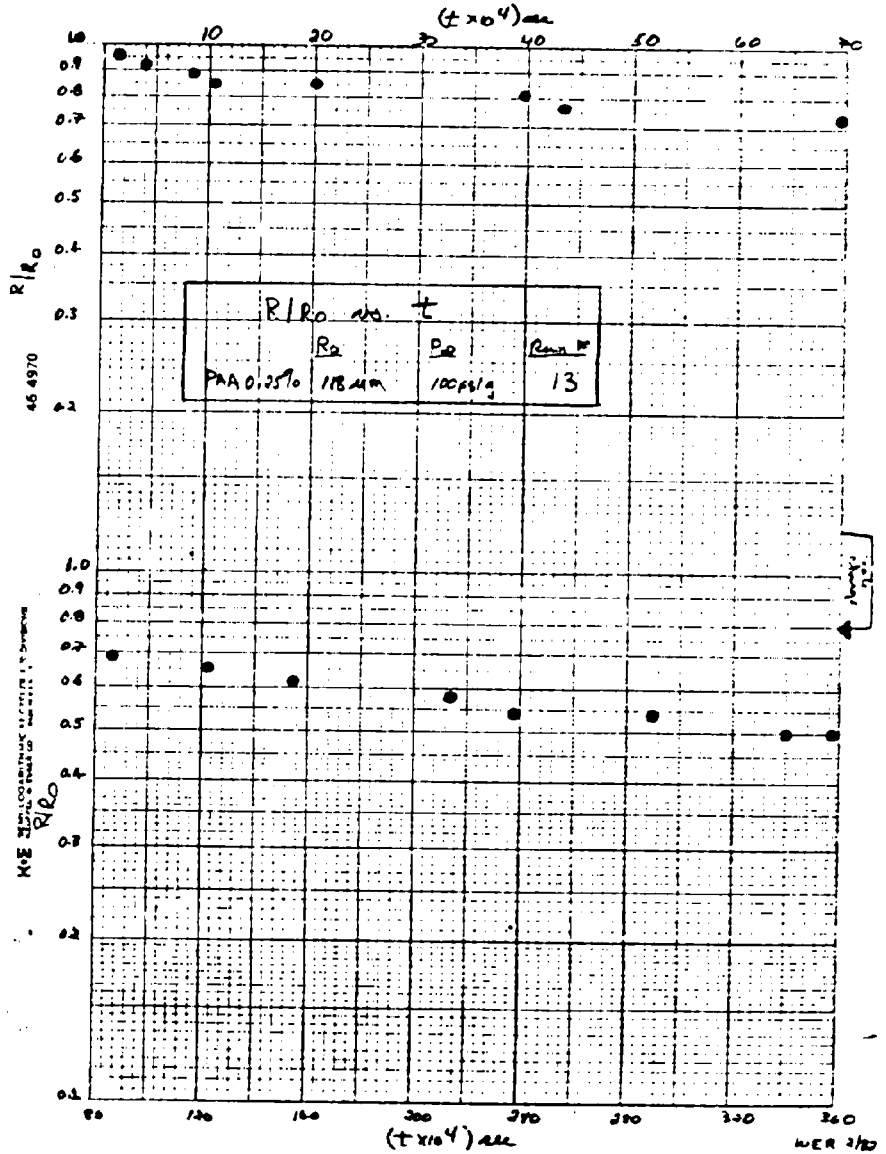
(t x10⁴) sec
R/Ro vs. t
Ro
Pa
Run #
PAA 0.25% 118 nm 100 psig 13
R/Ro
Scale Change
(t x10⁴) sec

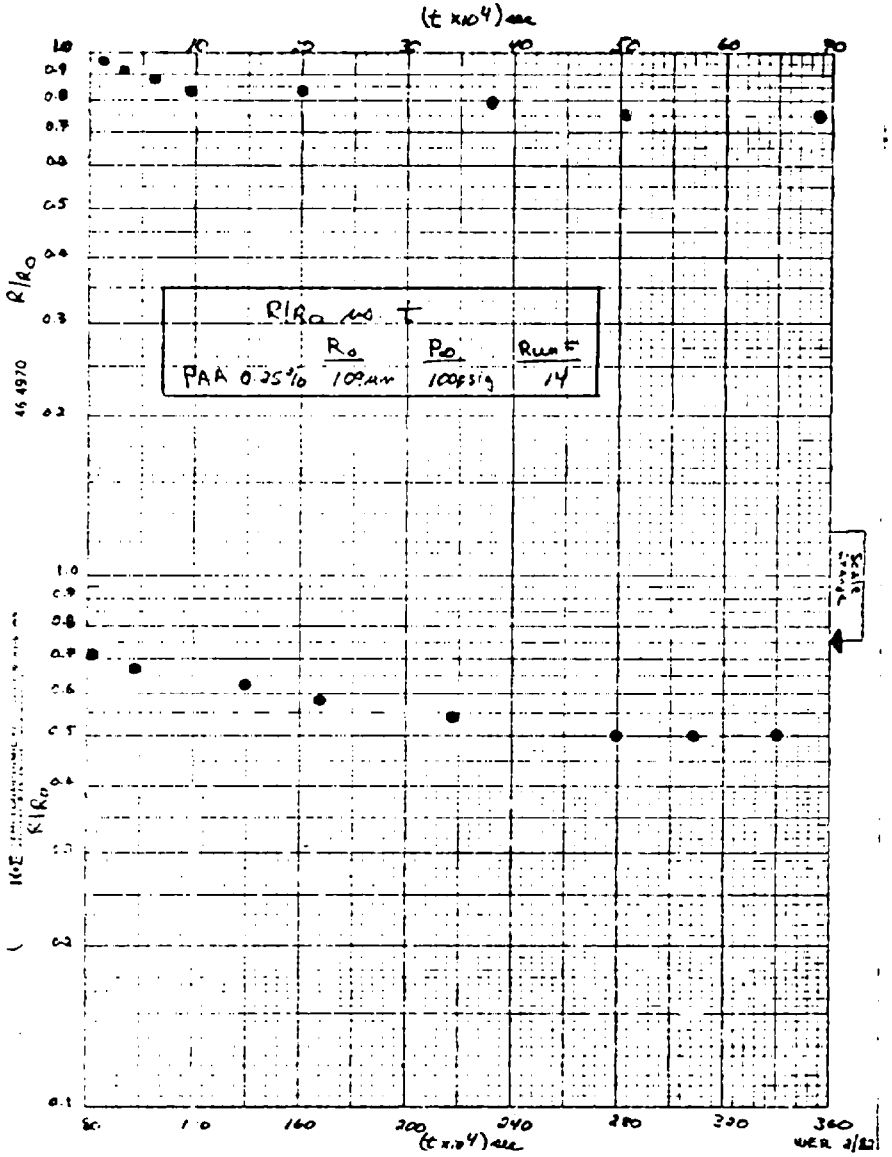
(t x10^4) sec
R/Ro
R/Ro vs t
PAA 0.25% Ro 100 mm Po 100 psig Run # 14
(t x10^4) sec

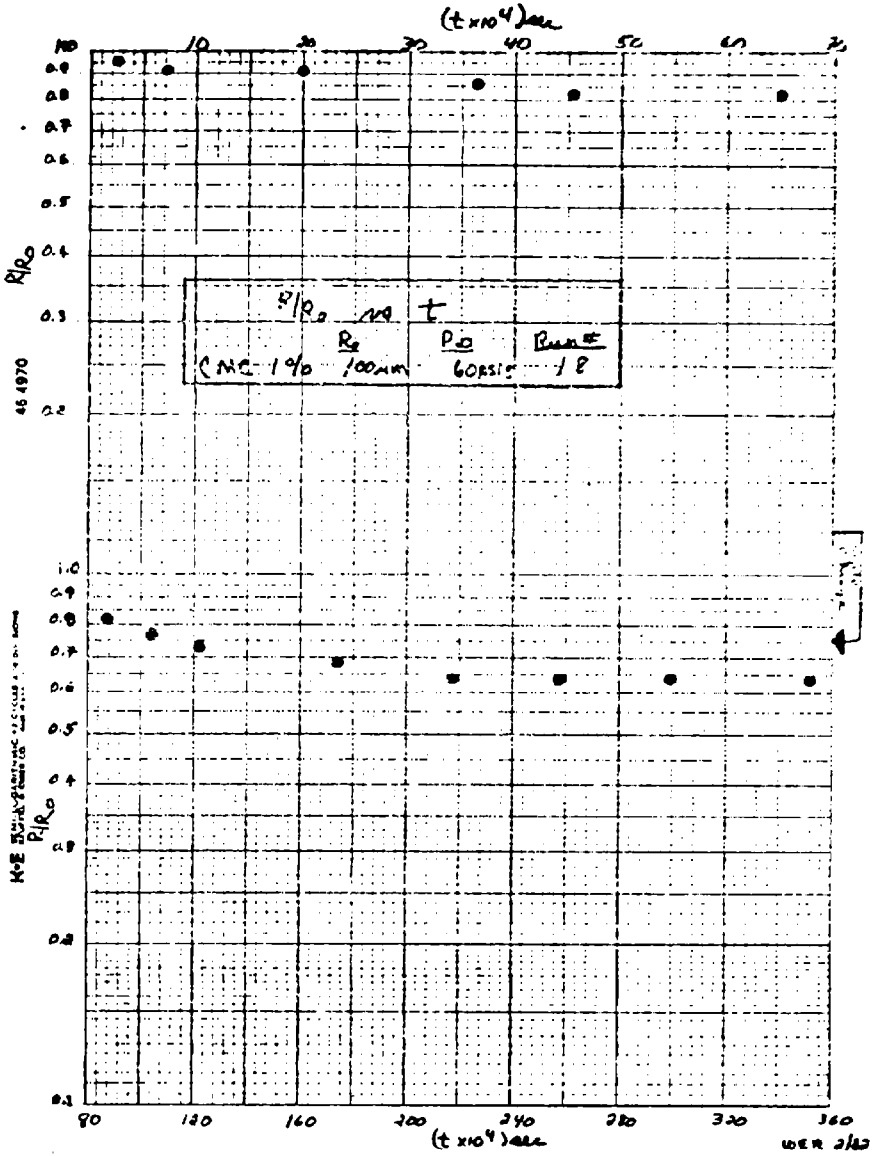
(t x10^4) sec
R/Ro
R/Ro vs t
CMC 1% Ro 100 mm Po 60 psig Run # 18
(t x10^4) sec

GLOSSARY

$Bo = g\rho r_o^2/\gamma$	Bond number
g	Acceleration of gravity
H	Disk thickness
M	Memory function
m	Heat capacity ratio
P_1	Increment in pressure causing collapse
P_G	Pressure inside the bubble
P_∞	External pressure on the fluid
p	Pressure distribution within fluid
r_o	Drop radius
R	Radius of bubble
r	Radial coordinate
$T = t/\lambda$	
t	Time variable
V	Volume of bubble
$\underline{v} = (v_r, v_\theta, v_z)$	Velocity vector
z	Axial coordinate
$\alpha = \frac{1}{2}\frac{(-\dot{H})}{H}$	
γ	Surface tension

$\underset{\sim}{\gamma}[o]$	Strain tensor
$\dot{\gamma}$	Shear rate
$\underset{\sim}{\Delta}$	Rate of deformation tensor
$\dot{\epsilon}_o = -\dot{H}/H$	
η	Nonnewtonian viscosity
λ	Relaxation time
$\Lambda = \lambda \dot{\epsilon}_o$	
μ	Newtonian viscosity
Π	Dimensionless pressure
ρ	Fluid density
$\underset{\sim}{\tau}$	Stress tensor

DISTRIBUTION LIST 4

Names	Copies
CHEMICAL SYSTEMS LABORATORY	
ATTN: DRDAR-CLB	1
ATTN: DRDAR-CLB-C	1
ATTN: DRDAR-CLB-PO	1
ATTN: DRDAR-CLB-PS	1
ATTN: DRDAR-CLB-R	1
ATTN: DRDAR-CLB-R(A)	1
ATTN: DRDAR-CLB-R(M)	1
ATTN: DRDAR-CLB-R(S)	1
ATTN: DRDAR-CLB-T	1
ATTN: DRDAR-CLB-TE	1
ATTN: DRDAR-CLC-B	1
ATTN: DRDAR-CLC-C	1
ATTN: DRDAR-CLC-E	1
ATTN: DRDAR-CLF	1
ATTN: DRDAR-CLJ-P	2
ATTN: DRDAR-CLJ-L	2
ATTN: DRDAR-CLJ-M	1
ATTN: DRDAR-CLN	1
ATTN: DRDAR-CLN-TE	1
ATTN: DRDAR-CLT	1
ATTN: DRDAR-CLW-C	1
ATTN: DRDAR-CLW-P	1
ATTN: DRDAR-CLW-E	1
ATTN: DRDAR-CLY-A	1
ATTN: DRDAR-CLY-R	4
COPIES FOR AUTHOR(S) Research Division (CPO)	6
RECORD COPY: DRDAR-CLB-A	1
DEPARTMENT OF DEFENSE	
Defense Technical Information Center ATTN: DTIC-DDA-2 Cameron Station, Building 5 Alexandria, VA 22314	2
Director Defense Intelligence Agency ATTN: DS-4G1 Washington, DC 20301	1
Commander USASED, USAINSCOM ATTN: IAFM-SED-III Fort Meade, MD 20755	1
DEPARTMENT OF THE ARMY	
HQDA ATTN: DAMO-NCC	1
ATTN: DAMO-NC/COL Robinson WASH DC 20310	1
Federal Emergency Management Agency Office of Research/NPP ATTN: David W. Bensen Washington, DC 20472	1
HQ DA Office of the Deputy Chief of Staff for Research, Development & Acquisition ATTN: DAMA-CSS-C Washington, DC 20310	1
HQ Sixth US Army ATTN: AFKC-OP-NBC Presidio of San Francisco, CA 94129	1
Commander DARCOM, STITEUR ATTN: DRXST-STI Box 48, APO New York 09710	1
Commander USASTCFEO ATTN: MAJ Mikeworth APO San Francisco 96328	1
HQ, 5th Infantry Division (Mech) ATTN: Division Chemical Officer Fort Polk, LA 71459	1

Commander
US Army Nuclear & Chemical Agency
ATTN: MONA-WE 1
7500 Backlick Rd, Bldg 2073
Springfield, VA 22150

Army Research Office
ATTN: DRXRO-CB (Dr. R. Ghirardelli) 1
P.O. Box 12211
Research Triangle Park, NC 27709

OFFICE OF THE SURGEON GENERAL

Commander
US Army Medical Bioengineering Research and Development Laboratory
ATTN: SGRD-UBD-AL, Bldg 568 1
Fort Detrick, Frederick, MD 21701

Commander
USA Medical Research Institute of Chemical Defense
ATTN: SGRD-UV-L 1
Aberdeen Proving Ground, MD 21010

US ARMY MATERIEL DEVELOPMENT AND READINESS COMMAND

Commander
US Army Materiel Development and Readiness Command
ATTN: DRCLDC 1
ATTN: DRCSF-P 1
5001 Eisenhower Ave
Alexandria, VA 22333

PM Smoke/Obscurants
ATTN: DROPM-SMK-S 3
Aberdeen Proving Ground, MD 21005

Commander
US Army Foreign Science & Technology Center
ATTN: DRXST-MT3 1
220 Seventh St., NE
Charlottesville, VA 22901

Director
US Army Materiel Systems Analysis Activity
ATTN: DRXSY-MP 1
ATTN: DRXSY-CA (Mr. Metz) 1
Aberdeen Proving Ground, MD 21005

Commander
US Army Missile Command
Redstone Scientific Information Center
ATTN: DRSMI-RPR (Documents) 1
Redstone Arsenal, AL 35809

Director
DARCOM Field Safety Activity
ATTN: DRXOS-C 1
Charlestown, IN 47111

Commander
US Army Natick Research and Development Laboratories
ATTN: DRDNA-O 1
ATTN: DRDNA-IC 1
ATTN: DRDNA-ICAA 1
ATTN: DRDNA-IM 1
ATTN: DRDNA-ITF (Dr. Roy W. Roth) 2
Natick, MA 01760

US ARMY ARMAMENT RESEARCH AND DEVELOPMENT COMMAND

Commander
US Army Armament Research and Development Command
ATTN: DRDAR-LCA-L 1
ATTN: DRDAR-LCU-CE 1
ATTN: DRDAR-NC (COL Lynn) 3
ATTN: DRDAR-SCM 1
ATTN: DRDAR-SCS 1
ATTN: DRDAR-TDC (Dr. D. Gyorog) 1
ATTN: DRDAR-TSS 2
ATTN: DRC[illegible] 1
Dover, NJ

US Army Armament Research and
Development Command

Resident Operations Office
ATTN: DRDAR-TSE-OA (Robert Thresher) 1
National Space Technology Laboratories
NSTL Station, MS 39529

Commander
ARRADCOM
ATTN: DRDAR-QAC-E 1
Aberdeen Proving Ground, MD 21010

Commander
USA Technical Detachment 1
US Naval EOD Technology Center
Indian Head, MD 20640

US ARMY ARMAMENT MATERIEL READINESS
COMMAND

Commander
US Army Armament Materiel Readiness Command
ATTN: DRSAR-ASN 1
ATTN: DRSAR-IRW 1
Rock Island, IL 61299

Commander
USA ARRCOM
ATTN: SARTE 1
Aberdeen Proving Ground, MD 21010

Commander
US Army Dugway Proving Ground
ATTN: Technical Library (Docu Sect) 1
Dugway, UT 84022

US ARMY TRAINING & DOCTRINE COMMAND

Commandant
US Army Infantry School
ATTN: CTDD, CSD, NBC Branch 1
Fort Benning, GA 31905

Commandant
US Army Missile & Munitions Center
and School
ATTN: ATSK-CM 1
ATTN: ATSK-TME 1
Redstone Arsenal, AL 35809

Commander
US Army Logistics Center
ATTN: ATCL-MG 1
Fort Lee, VA 23801

Commandant
US Army Chemical School
ATTN: ATZN-CM-C 1
ATTN: ATZN-CM-AD 2
ATTN: ATZN-CM-TPC 2
Fort McClellan, AL 36205

Commander
USAAVNC
ATTN: ATZQ-D-MS 1
Fort Rucker, AL 36362

Commander
US Army Infantry Center
ATTN: ATSH-CD-MS-C 1
Fort Benning, GA 31905

Commander
US Army Infantry Center
Directorate of Plans & Training
ATTN: ATZB-DPT-PO-NBC 1
Fort Benning, GA 31905

Commander
USA Training and Doctrine Command
ATTN: ATCD-N 1
Fort Monroe, VA 23651

Commander
US Army Armor Center
ATTN: ATZK-CD-MS 1
ATTN: ATZK-PPT-PO-C 1
Fort Knox, KY 40121

Commander
USA Combined Arms Center and
Fort Leavenworth
ATTN: ATZL-CAM-IM 1
Fort Leavenworth, KS 66027

US ARMY TEST & EVALUATION COMMAND

Commander
US Army Test & Evaluation Command
ATTN: DRSTE-CM-F 1
ATTN: DRSTE-CT-T 1
Aberdeen Proving Ground, MD 21005

DEPARTMENT OF THE NAVY

Project Manager
Theatre Nuclear Warfare Project Office
ATTN: TN-09C 1
Navy Department
Washington, DC 20360

Chief of Naval Research
ATTN: Code 441 1
800 N. Quincy Street
Arlington, VA 22217

Commander
Naval Explosive Ordnance Disposal
Technology Center
ATTN: AC-3 1
Indian Head, MD 20640

Officer-in-Charge
Marine Corps Detachment 1
Naval Explosive Ordnance Disposal
Technology Center
Indian Head, MD 20640

Commander
Naval Surface Weapons Center
Code G51 1
Dahlgren, VA 22448

Chief, Bureau of Medicine & Surgery
Department of the Navy
ATTN: MED 3C33 1
Washington, DC 20372

Commander
Naval Air Development Center
ATTN: Code 2012 (Dr. Robert Helmbold) 1
Warminster, PA 18974

US MARINE CORPS

Commandant
HQ, US Marine Corps
ATTN: Code LMW-50 1
Washington, DC 20380

Commanding General
Marine Corps Development and
Education Command
ATTN: Fire Power Division, D091 1
Quantico, VA 22134

DEPARTMENT OF THE AIR FORCE

ASD/AESD 1
Wright-Patterson AFB, OH 45433

HQ AFSC/SDZ 1
ATTN: CPT D. Riediger
Andrews AFB, MD 20334

HQ, AFSC/SDNE 1
Andrews AFB, MD 20334

HQ, AFSC/SGB 1
Andrews AFB, DC 20334

HQ, NORAD
ATTN: J-3TU 1
Peterson AFB, CO 80914

AFAMRL/HE
ATTN: Dr. Clyde Repoggle 1
Wright-Patterson AFB, OH 45433

HQ AFTEC/TEL 1
Kirtland AFB, NM 87117

USAF TAWC/THL 1
Eglin AFB, FL 32542

AFATL/DLV 1
Eglin AFB, FL 32542

USAF SC
ATTN: AD/YQ 1
ATTN: AD/YQO (MAJ Owens) 1
Eglin AFB, FL 32542

USAFSAM/VN
Deputy for Chemical Defense
ATTN: Dr. F. Wesley Baumgardner 1
Brooks AFB, TX 78235

AFAMRL/TS
ATTN: COL Johnson 1
Wright-Patterson AFB, OH 45433

AMD/RDTK
ATTN: LTC T. Kingery 1
Brooks AFB, TX 78235

AMD/RDSM 1
Brooks AFB, TX 78235

AMD/RDSX 1
Brooks AFB, TX 78235

AD/XRO 1
Eglin AFB, FL 32542

OUTSIDE AGENCIES

Battelle, Columbus Laboratories
ATTN: TACTEC 1
505 King Avenue
Columbus, OH 43201

Toxicology Information Center, JH 652
National Research Council 1
2101 Constitution Ave., NW
Washington, DC 20418

US Public Health Service
Center for Disease Control
ATTN: Lewis Webb, Jr. 1
Building 4, Room 232
Atlanta, GA 30333

Director
Central Intelligence Agency
ATTN: AMR/ORD/DD/S&T 1
Washington, DC 20505

ADDITIONAL ADDRESSEES

Commandant
Academy of Health Sciences, US Army
ATTN: HSHA-CDH 1
ATTN: HSHA-IPM 2
Fort Sam Houston, TX 78234